processes

MDPI

Article

The Calibrated Safety Constraints Optimal Power Flow for the Operation of Wind-Integrated Power Systems

Kai-Hung Lu [1,2], Wenjun Qian [1,*], Yuesong Jiang [1,3,*] and Yi-Shun Zhong [4]

[1] School of Electronic and Electrical Engineering, Minnan University of Science and Technology, Quanzhou 362700, China; khluphd@gmail.com
[2] Key Laboratory of Industrial Automation Control Technology and Application of Fujian Higher Education, Quanzhou 362700, China
[3] School of Electronic and Information Engineering, Beihang University, Beijing 100191, China
[4] Department of Electrical Engineering, National Sun Yat-Sen University, Kaohsiung 80424, Taiwan; no07210815@icloud.com
* Correspondence: wiqwiq20@126.com (W.Q.); yuesongjiang@vip.sina.com (Y.J.)

Abstract: As the penetration of renewable energy sources (RESs), particularly wind power, continues to rise, the uncertainty in power systems increases. This challenges traditional optimal power flow (OPF) methods. This paper proposes a Calibrated Safety Constraints Optimal Power Flow (CSCOPF) model that uses the Improved Acceleration Coefficient-Based Bee Swarm algorithm (IACBS) in combination with the equivalent current injection (ECI) model. The proposed method addresses key challenges in wind-integrated power systems by ensuring preventive safety scheduling and enabling effective power incident safety analysis (PISA). This improves system reliability and stability. This method incorporates mixed-integer programming, with continuous and discrete variables representing power outputs and control mechanisms. Detailed numerical simulations were conducted on the IEEE 30-bus test system, and the feasibility of the proposed method was further validated on the IEEE 118-bus test system. The results show that the IACBS algorithm outperforms the existing methods in both computational efficiency and robustness. It achieves lower generation costs and faster convergence times. Additionally, the CSCOPF model effectively prevents power grid disruptions during critical incidents, ensuring that wind farms remain operational within predefined safety limits, even in fault scenarios. These findings suggest that the CSCOPF model provides a reliable solution for optimizing power flow in renewable energy-integrated systems, significantly contributing to grid stability and operational safety.

Keywords: load flow control; power incident safety analysis (PISA); renewable energy sources (RESs); improved acceleration coefficient-based bee swarm (IACBS)

Citation: Lu, K.-H.; Qian, W.; Jiang, Y.; Zhong, Y.-S. The Calibrated Safety Constraints Optimal Power Flow for the Operation of Wind-Integrated Power Systems. *Processes* **2024**, *12*, 2272. https://doi.org/10.3390/pr12102272

Academic Editor: Takuya Oda

Received: 29 September 2024
Revised: 10 October 2024
Accepted: 15 October 2024
Published: 17 October 2024

1. Introduction

Wind energy generation is highly random and intermittent. As wind farms are integrated into the power grid and their scale expands, this integration will inevitably impact the operation of the power system [1]. This impact is significant across various aspects, with the power dispatch of grid-connected wind farms being a basic critical issue. Inaccuracies in wind power output forecasts and accidents in the power grid often cause wind curtailment during dispatch [2]. Thus, solving this issue is fundamental for further research on related topics. A key challenge is how to establish an optimized power dispatch with preventive safety restrictions so that if a power system with a high proportion of wind energy generation experiences a failure—especially in the most serious case—the grid dispatcher does not need to make any dispatch changes, and the system can still operate safely within limits.

The intermittent nature of renewable energy generation poses challenges to power grid stability, as sudden fluctuations in power generation can impact the system. Without

proper auxiliary services, these fluctuations can result in outages or even system collapse. Yunus et al. [3] have focused on the impact of offshore wind farms, while Li et al. [4] introduced a linear optimal power flow model for renewable energy integration. Recent developments, such as the data-driven linear optimal power flow model, have been shown to improve accuracy in distribution networks with high renewable energy penetration. For example, Yunus et al. [3] and Li et al. [4] address uncertainty but fail to consider non-linear dynamics in large-scale grids. Amr et al. [5] propose a stochastic optimal power flow approach using the heuristic method Aquila Optimizer (AO) to optimize wind farm scheduling and minimize total operating costs. Li [6] introduces an improved adaptive Differential Evolution (DE) approach with a penalty constraint handling strategy to address optimal power flow (OPF) challenges in an IEEE-30 bus system. Meanwhile, Amr et al. [5] and Li et al. [6] present heuristic solutions that, while effective in small to medium systems, might struggle with robustness in larger, more complex networks. Khan [7] presents a heuristic algorithm aimed at efficiently solving the optimal power flow problem while incorporating stochastic renewable energy sources. However, as noted by Khan et al. [7], stochastic methods bring their own set of limitations, including potential difficulties in guaranteeing robustness. Although these studies provide valuable insights, they often have limitations. For example, ref. [8] proposes a robust OPF (RACOPF) model based on robust optimization (RO) for power grids with uncertain wind power, achieving lower expected power generation costs compared to AAROPF by employing second-order programming techniques to transform RACOPF into a mixed-integer SOCP (MISOCP) model. While ref. [8] offers a robust optimization framework, it relies on simplifying assumptions that may not capture the full complexity of wind power variability in larger systems. Additionally, the existing OPF models often overlook the mutual coupling effect, which Chowdhury [9] addresses by proposing an AC-OPF model for three-phase radial distribution networks based on second-order cone programming (SOCP). While these models primarily focus on steady-state conditions, they do not directly consider potential accidents or the dynamic behavior of the grid during faults [10].

Morshed et al. [11] proposed a probabilistic multi-objective approach for wind-PV-PEV systems, effectively handling uncertainty, but overlooked real-world power flow instability. Shi et al. [12] included wind power in OPF, though it did not address the complexity of large-scale grids. Momoh et al. [13] reviewed non-linear OPF methods, but their high computational complexity limits modern application. Pourakbari-Kasmaei et al. [14] introduced a MINLP model for constrained OPF, though it may struggle with efficiency in large grids. Cheng et al. [15] and Tang et al. [16] expanded MAS control under uncertain conditions but face scalability issues. Ben Hmida et al. [17] used hybrid algorithms for OPF in wind–solar systems, showing potential but requiring validation in dynamic environments. Cheng et al. [18,19] proposed control strategies for systems with hysteresis, though practical application remains untested. Avvari and DM [20] offered a hybrid algorithm for OPF in renewable systems, effective in multi-objective cases but needing refinement for real-world complexity. Abd-El Wahab et al. [21] and Deb et al. [22] explored turbulent flow optimization for reactive power dispatch, effective in economic dispatch, yet lacking comparison with other algorithms, particularly in dynamic settings.

In general, the conventional Newton–Raphson method is widely and extensively utilized to address load flow issues in power systems, regardless of considerations such as grid safety correction. A conic quadratic format has also been proposed to improve the load flow equations for meshed networks, which simplifies some computational complexities [23]. The partial differentiation of bus voltage and angle is executed based on power, serving as the slope of the approaching system solution. However, the resulting Jacobian matrix is not constant. Consequently, during each iteration, all the elements in the Jacobian matrix need to be updated and adjusted, necessitating a redo of the LU decomposition. When dealing with large systems, this entire load flow-solving process becomes exceedingly time-consuming and intricate. Load flow techniques based on the equivalent current injection (ECI) method have been successfully devised and applied in three-phase unbalanced

systems [24]. Various decoupling laws have been formulated to cater to different characteristics of the power system and can be implemented across different systems. Additionally, a Gaussian Process Learning-Based Probabilistic Optimal Power Flow model has been proposed to enhance the handling of uncertainties and improve computational efficiency in large-scale systems [25]. The Jacobian matrix derived for load buses (PQ buses) in the ECI-power flow method remains constant and independent of the system state, requiring no updates to its elements during iteration. Additionally, the Jacobian matrix obtained for voltage buses (PV buses) only necessitates modifications to a small number of elements in each iteration, leading to significantly reduced solving time. Consequently, this method exhibits excellent convergence properties, rapid decoupling characteristics, and minimal memory requirements. Although the current injection network model can address speed issues on a large scale, many studies have found the integer programming solutions for control variables (discrete variables) to be unsatisfactory [26,27].

In recent years, numerous intelligent algorithms have been developed and applied to the scheduling issues of power systems. Genetic Algorithm (GA) optimizes wind and thermal dispatch to cut costs, considering wind variability and thermal constraints [28]. One article [29] discusses the application of a developed Grey Wolf Optimizer (GWO) to solve non-smooth optimal power flow problems in energy systems. In [29], while effective in solving non-smooth OPF problems, it may struggle with convergence speed and risks getting trapped in local minima, especially in larger and more complex systems. Salkuti [30] explores the use of a Multi-Objective Glowworm Swarm Optimization Algorithm (GSO) for optimizing power flow in a power system integrated with wind energy. Furthermore, the Glowworm Swarm Optimization algorithm discussed in [30], despite its multi-objective capabilities, is highly sensitive to parameter tuning, and its performance can degrade significantly if not properly calibrated for different system conditions. Both methods could benefit from enhanced robustness to handle more diverse and dynamic grid environments. Pham [31] introduces a Multi-Objective Coronavirus Herd Immunity Algorithm (CHI) to address these aspects. This innovative approach aims to optimize the performance of power networks by balancing costs. However, while the CHI algorithm brings novelty in mimicking herd immunity strategies, it may face challenges in efficiently handling the high-dimensional search spaces found in complex power systems, potentially leading to slower convergence rates. Ahmad [32] presents a study on solving the optimal power flow problem within a hybrid power system using a bio-inspired heuristic algorithm (BIH). Although the BIH algorithm is effective in hybrid systems, it remains sensitive to initial parameter settings, and its ability to maintain global optimality in diverse operating conditions remains uncertain, particularly when applied to larger grid structures.

Despite the advances in related research, many shortcomings and technical bottlenecks still need to be overcome. For instance, the safety planning for the stable operation of power grids containing renewable energy has not been fully considered in the event of a fault. The process of solving the power flow method is both time-consuming and complicated, and discrete variable issues persist in the power grid. Moreover, even when intelligent algorithms are used to solve discrete problems, they are prone to falling into local optima. These urgent problems need to be addressed. Therefore, this paper proposes a Calibrated Safety Constraints Optimal Power Flow (CSCOPF) and applies the Improved Acceleration Coefficient-Based Bee Swarm Algorithm (IACBS) to solve the optimal power flow problem based on the ECI model, combined with calibrated safety constraints. This safety dispatch strategy includes planning the system before accidents occur and establishing new power incident safety analysis (PISA) protocols for the grid to identify and categorize all the vulnerable parts of the system circuit based on power flow results, and to make safe arrangements for the most severe incidents. In the event of an accident, it ensures that the illegal operations of the power grid, including wind farms, can be avoided without making any dispatch changes, allowing the system to operate safely within limits.

This study introduces a novel calibrated safety constraint mechanism, which enhances the system's reliability by ensuring that it operates within safety limits even under severe

fault conditions. Unlike previous OPF models, this approach addresses both the preventive and real-time stability of wind-integrated power systems. In addition, compared to traditional algorithms like GA and PSO, IACBS provides faster convergence and more effectively avoids the local optima, particularly in non-linear and complex systems. This study demonstrates the superior performance of IACBS in large-scale wind-integrated power systems, highlighting its ability to offer a more robust and efficient optimization solution.

To address these challenges, this paper proposes a novel approach with two key innovations. The first is the Calibrated Safety Constraints Optimal Power Flow (CSCOPF) model, which enhances system reliability by incorporating calibrated safety constraints to manage uncertainties during severe faults. Unlike traditional methods that primarily focus on steady-state conditions, this approach addresses both preventive and real-time stability, offering a robust solution for wind-integrated power systems. The second innovation is the Improved Acceleration Coefficient-Based Bee Swarm Algorithm (IACBS), which significantly improves optimization performance in non-linear and complex systems. Compared to traditional algorithms like GA and PSO, IACBS provides faster convergence and more effectively avoids local optima, demonstrating superior efficiency in large-scale systems. These innovations contribute both theoretically and practically by enhancing system stability and reliability while addressing the existing research gaps.

2. Mathematical Model of CSCOPF

This section details the mathematical formulation of the CSCOPF model. The CSCOPF model aims to optimize power flow while incorporating safety constraints to manage system uncertainties effectively. The model uses the IACBS for optimization and the current injection method for load flow constraints.

2.1. Load Flow Model Using ECI Method

The ECI method is utilized to solve load flow problems in transmission systems, building on its successful application in distribution systems with three-phase unbalanced loads. This section integrates the ECI method with the Newton–Raphson approach for efficient load flow analysis.

A. Transmission line representation:

A transmission line connecting bus S to bus R is represented using a π model, as shown in Figure 1. The resistance R_{SR} and inductance L_{SR} of the line are represented by the transmission admittance $G_{SR} + jB_{SR}$. The line's capacitance C_T to ground is associated with a susceptance jB_C. The equivalent current injected at bus S is given by the following [24]:

$$I_S(k) = \frac{-S_S}{U_S(k)^*} = I_{S,r}(k) + jI_{S,i}(k) \quad (1)$$

where S_S refers to the complex power injection at bus S, and U_S denotes the corresponding terminal voltage. The superscript k indicates the iteration step, with r and i signifying the real and imaginary parts, respectively.

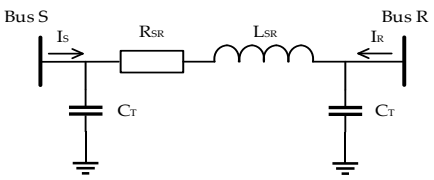

Figure 1. Transmission line equivalent π model.

B. Rectangular coordinate form:

The rectangular coordinate form of the currents I_S and I_R injected at bus S is as follows:

$$\begin{aligned} I_S = {} & [G_{SR}(U_{S,r} - U_{R,r}) - B_{SR}(U_{S,i} - U_{R,i}) - B_C U_{S,i}] \\ & + j[G_{SR}(U_{S,i} - U_{R,i}) - B_{SR}(U_{S,r} - U_{R,r}) + B_C U_{S,r}] \end{aligned} \tag{2}$$

$$\begin{aligned} I_R = {} & [G_{SR}(U_{R,r} - U_{S,r}) - B_{SR}(U_{R,i} - U_{S,i}) - B_C U_{R,i}] \\ & + j[G_{SR}(U_{R,i} - U_{S,i}) - B_{SR}(U_{R,r} - U_{S,r}) + B_C U_{R,r}] \end{aligned} \tag{3}$$

Then, separate the complex currents I_S and I_R into their respective real ($I_{S,r}$, $I_{R,r}$) and imaginary ($I_{S,i}$, $I_{R,i}$) components. This allows us to express the current Equations (1)–(3) in a form compatible with the Newton–Raphson method. Specifically, by linearizing these equations and calculating the partial derivatives with respect to the state variables $U_{S,r}$, $U_{S,i}$, $U_{R,r}$, and $U_{R,i}$, we obtain the following Jacobian matrix:

$$\begin{aligned} \Delta I_r(k) &= J_{11}\Delta U_r + J_{12}\Delta U_i \\ \Delta I_i(k) &= J_{21}\Delta U_r + J_{22}\Delta U_i \end{aligned} \tag{4}$$

where the Jacobian matrix elements J_{ij} are constant and determined by the admittance matrix between buses S and R.

For Equations (2) and (3), take partial derivatives with respect to the state variables $U_{S,r}$, $U_{S,i}$, $U_{R,r}$, and $U_{R,i}$. The organized error equations are as follows:

$$\begin{aligned} \begin{bmatrix} \Delta I_{S,r} \\ \Delta I_{R,r} \\ \Delta I_{S,i} \\ \Delta I_{R,i} \end{bmatrix} &= \begin{bmatrix} G_{SR} & -G_{SR} & -(B_{SR}+B_C) & B_{SR} \\ -G_{SR} & G_{SR} & B_{SR} & -(B_{SR}+B_C) \\ (B_{SR}+B_C) & -B_{SR} & G_{SR} & -G_{SR} \\ -B_{SR} & (B_{SR}+B_C) & -G_{SR} & G_{SR} \end{bmatrix} \begin{bmatrix} \Delta U_{S,r} \\ \Delta U_{R,r} \\ \Delta U_{S,i} \\ \Delta U_{R,i} \end{bmatrix} \\ &= [J_{SR}] \begin{bmatrix} \Delta U_r \\ \Delta U_i \end{bmatrix} \end{aligned} \tag{5}$$

From Equation (5), it becomes clear that the matrix functions as the Jacobian matrix during the iterations, with its elements directly corresponding to the admittance matrix between buses S and R.

C. Jacobian Matrix Efficiency:

The Jacobian matrix's constancy across iterations provides significant computational efficiency, as it avoids recalculation at each iteration. This constant nature simplifies the load flow solution process, leading to faster convergence and reduced computational time.

$$\begin{bmatrix} \Delta I_r(k) \\ \Delta I_i(k) \end{bmatrix} = \begin{bmatrix} y_G & -y_B \\ y_B & y_G \end{bmatrix} \begin{bmatrix} \Delta U_r(k) \\ \Delta U_i(k) \end{bmatrix} \tag{6}$$

D. Voltage Control Buses:

In a power system, generator buses (PV buses), which typically include independent generators or wind generators, are integral components. However, the approach to deriving the parameters for these voltage buses differs from that used for the load buses previously discussed. When attempting to model these PV buses as current sources, challenges arise in integrating the known parameters with the established load flow model. Consequently, it is crucial to address the specific issues related to voltage buses within the framework of the equivalent current injection method and to harmonize these with the previously developed load bus model in order to create a comprehensive power system load flow model. To resolve the challenges associated with PV buses in the equivalent current injection approach, the real power injection at a PV bus can be expanded using a Taylor series, resulting in the following:

$$\Delta P_S = U_r \cdot \Delta I_{S,r} + U_i \cdot \Delta I_{S,i} + \Delta U_r \cdot I_{S,r} + \Delta U_i \cdot I_{S,i} \tag{7}$$

Substituting Equation (5) into Equation (7) and rearranging gives Equation (8):

$$\begin{aligned}\Delta P_S = &\left(U_{S,r}G_{SR}+U_{S,i}B'_{SR}+I_{S,r}\right)\Delta U_{S,r}+\left(-U_{S,r}B'_{SR}+U_{S,i}G_{SR}+I_{S,i}\right)\Delta U_{S,i}\\ &+\left(-U_{S,r}G_{SR}-U_{S,i}B_{SR}\right)\Delta U_{R,r}+\left(U_{S,r}B_{SR}-U_{S,i}G_{SR}\right)\Delta U_{R,i}\end{aligned} \tag{8}$$

where $B'_{SR} = B_{SR} + B_C$.

Then, performing a Taylor expansion on the generator terminal voltage $|U_S|^2 = U_{S,r}^2 + U_{S,i}^2$ yields the following:

$$\Delta|U_S|^2 = 2U_{S,r}\Delta U_{S,r} + 2U_{S,i}\Delta U_{S,i} \tag{9}$$

By reorganizing Equations (8) and (9), one can derive the Jacobian matrix associated with voltage control buses, as well as the corresponding error equation, as depicted in Equation (10).

$$\begin{bmatrix}\Delta P_S\\ \Delta|U_S|^2\end{bmatrix} = \begin{bmatrix}J_1 & J_2\\ J_3 & J_4\end{bmatrix}\begin{bmatrix}\Delta U_{S,r}\\ \Delta U_{S,i}\\ \Delta U_{R,r}\\ \Delta U_{R,i}\end{bmatrix} \tag{10}$$

where $J_1 = \left[(U_{S,r}G_{SR}+U_{S,i}B'_{SR}+I_{S,r})(-U_{S,r}G_{SR}-U_{S,i}B_{SR})\right]$, $J_2 = [(-U_{S,r}B'_{SR}+U_{S,i}G_{SR} + I_{S,i})(U_{S,r}B_{SR}-U_{S,i}G_{SR})]$, $J_3 = [2U_{S,r}0]$, and $J_4 = [2U_{S,i}0]$.

Using the above formula, calculate P and V to replace the left-hand side of Equation (5), thus forming a complete load flow error equation, as shown in Equation (11).

$$\begin{bmatrix}\Delta I_{1,r}\\ \vdots\\ \Delta P_S\\ \vdots\\ \Delta I_{M,r}\\ \hline \Delta I_{1,i}\\ \vdots\\ \Delta|U_S|^2\\ \vdots\\ \Delta I_{M,i}\end{bmatrix} = \left[\begin{array}{ccc:ccc} & & & & & \\ & & & & & \\ & J_{Gr} & & & J_{Br} & \\ & & & & & \\ & & & & & \\ \hdashline & & & & & \\ & & & & & \\ & J_{Bi} & & & J_{Gi} & \\ & & & & & \\ & & & & & \end{array}\right]\begin{bmatrix}\Delta U_{1,r}\\ \vdots\\ \Delta U_{S,r}\\ \vdots\\ \Delta U_{M,r}\\ \hline \Delta U_{1,r}\\ \vdots\\ \Delta|U_S|^2\\ \vdots\\ \Delta I_{M,i}\end{bmatrix} \tag{11}$$

From Equation (11), in an M-bus system, when voltage control buses with wind turbines and synchronous generators are introduced, the corresponding elements in the Jacobian matrix must be updated during each iteration, rendering the matrix non-constant. However, the number of elements requiring modification in this Jacobian matrix is fewer compared to those in the traditional Newton–Raphson method. This is because although the Jacobian matrix needs to be revised at each iteration, only the elements associated with the voltage control buses require adjustment. This selective modification approach reduces the computational burden, as only a small subset of the matrix is recalculated, leading to faster convergence compared to the full matrix updates required in the traditional method.

2.2. Power Incident Safety Analysis (PISA)

The safety analysis involves simulating faults and adjusting the admittance matrix accordingly. This section describes the modification of the admittance matrix for fault scenarios. During the safety analysis of a system, simulating a specific fault requires reasonable adjustments to the model affecting the system while maintaining its original features unchanged. However, reconstructing the admittance matrix for all the components

of the system for each fault would be time-consuming. Therefore, this document adopts a method of directly modifying parts of the original admittance matrix related to the fault model, thus avoiding extensive time spent on revising the system model. The fault modification model is primarily divided into two parts for discussion: one is the generator trip incidents, and the other is the transmission line trip incidents.

2.2.1. Generator Trip Incident Correction Model

When a generator trips, the affected bus becomes a PQ bus. Other generators adjust to maintain system balance. At this time, in addition to the generators on the swing bus automatically maintaining the system's supply–demand balance by changing their power output, other generators continue to maintain their original real power output and generator bus voltage values.

$$P_{G\_fault} = P_{G|0|} + \Delta P_G \tag{12}$$

$$\Delta P_G = -P_{G|0|} \tag{13}$$

where $P_{G|0|}$ represents the generator output before the incident, P_{G_fault} is the remaining generator output after the incident, and ΔP_G is the real power correction amount in the system following the generator trip.

2.2.2. Transmission Line Trip Incident Correction Model

When a transmission line trips, the admittance matrix is updated. Assuming the line admittance from bus m to bus n is $[Y_{mn}]$, when this line trips

$$[Y_{mn}] = \begin{bmatrix} G_{mn} + j(B_{mn} - B_C) & -(G_{mn+}jB_{mn}) \\ -(G_{mn+}jB_{mn}) & G_{mn} + j(B_{mn} - B_C) \end{bmatrix} \tag{14}$$

$$\left[Y_{fault}\right] = \left[Y_{|0|}\right] + [\Delta Y_{mn}] \tag{15}$$

$$[\Delta Y_{mn}] = \begin{bmatrix} \ddots & & \iddots \\ \cdots \Delta Y_{mm} \cdots & & \cdots \Delta Y_{nm} \cdots \\ \vdots & \ddots & \vdots \\ \cdots \Delta Y_{nm} \cdots & & \cdots \Delta Y_{nn} \cdots \\ \iddots & & \ddots \end{bmatrix} \tag{16}$$

where $\left[Y_{|0|}\right]$ is the system admittance matrix before the incident, and $\left[Y_{fault}\right]$ is the system admittance matrix after the incident. $\Delta Y_{mm} = \Delta Y_{nn} - (G_{mn+}jB_{mn})$, $\Delta Y_{mm} = G_{mn+}jB_{mn}$.

3. CSCOPF Problem

3.1. Objective Functions

The OPF problem in power systems involves adjusting variables such as voltage levels and power outputs to manage the system efficiently within its physical and thermal constraints. This non-linear constrained optimization challenge is akin to solving a complex puzzle, where each component—such as generators and transmission lines—must operate within specific operational and safety limits to prevent system overload and ensure optimal performance.

This paper tackles the OPF problem using the ECI approach. It starts by assuming that the active power generation of wind turbines is non-dispatchable, and these quantities are treated as expected values within the framework of total power factor management. If the mean value of the uncertainty in the prediction error for the real power generation of each wind farm is zero, OPF operations are conducted precisely at predetermined ten-minute intervals [32]. Consequently, the voltage levels at the wind turbine (WT) bus are expected

to have a significant impact on OPF results. To further elucidate this point, a representative mathematical equation is introduced [32].

Objective function:

$$F_C(P_{g_j}) = \sum_{j \in g_j}^{n_g} A_j P_{g_j}^2 + B_j P_{g_j} + C_j \tag{17}$$

where P_{g_j} is the schedulable real power from the jth thermal power plant, while A_j, B_j, and C_j are the cost coefficients associated with the power output of that specific plant.

3.2. Equality and Inequality Constraints

The goal of OPF is to minimize the objective function while satisfying the following constraints:

A. Equality constraints:

The goal of OPF is to minimize Equation (17) under the conditions of equality constraint (18)–(21):

$$-I_{des\_r} + I_{com\_r} = 0 \tag{18}$$

$$-I_{des\_i} + I_{com\_i} = 0 \tag{19}$$

$$-P_{des\_gen} + P_L + P_{com\_gen} = 0 \tag{20}$$

$$-|U_{des}|^2 + |U_{com}|^2 \tag{21}$$

where I_{des_r} and I_{des_i} refer to the real and imaginary components of the designated equivalent current injections, whereas I_{coml_r} and I_{com_i} refer to the real and imaginary components of the currents as computed. P_{com_gen} and $|U_{com}|^2$ represent the calculated real power injection and the generator terminal voltage at the PV bus, respectively. P_{des_gen} and P_L represent the real power output of the generator and the real power load on the PV Bus. $|U_{des}|^2$ is the square of the absolute value of the voltage on the PV bus.

And

$$I_{des\_r} = \frac{P \cdot U_r + Q \cdot U_i}{U_r^2 + U_i^2} \tag{22}$$

$$I_{des\_i} = \frac{P \cdot U_i + Q \cdot U_r}{U_r^2 + U_i^2} \tag{23}$$

where U_r and U_i are the real and imaginary components of the bus voltage, respectively, while P and Q correspond to the real and reactive power associated with the equivalent injected at the load bus.

B. Inequality constraints:

$$S_{SR}^2 \le \overline{S}_{SR}^2 \tag{24}$$

$$S_{RS}^2 \le \overline{S}_{RS}^2 \tag{25}$$

$$\underline{P_{g_j}} \le P_{g_j} \le \overline{P_{g_j}} \tag{26}$$

$$\left|\underline{U_j}\right|^2 \le \left(U_{j,r}^2 + U_{j,i}^2\right) \le |\overline{U_j}|^2 \tag{27}$$

where $\left|\underline{U_j}\right|^2$ and $|\overline{U_j}|^2$, respectively, represent the lower and upper limits of the voltage magnitude at bus j; $\underline{P_{g_j}}$ and $\overline{P_{g_j}}$ are the lower and upper limits of the schedulable real power at bus j; (S, R) denotes the transmission line connecting bus S and bus R; S_{SR}^2 and S_{RS}^2 indicate the apparent power on the transmission line (S, R) or (R, S); $\overline{S}_{SR}^2$ and $\overline{S}_{RS}^2$ are the

upper limits of the apparent power on the transmission line (S, R) or (R, S), where $\overline{S}_{SR}^2$ is equal to $\overline{S}_{RS}^2$.

This paper introduces a continuous variable-type OPF with control variables consisting of the schedulable real power output of any generator P_{g_j} ($j = 1: n_g$) and generator voltage (WT)$|U_j|$ ($j = 1: n_g$), and state variables being the real and imaginary parts of bus voltages (U_r, U_i). The inequality constraints include generator and WT real power limits, bus voltage limits, and transmission line capacity limits. This OPF, which omits fault analysis and does not address integer issues, is classified as a continuous non-linear problem. The mixed-integer programming problem presented in this paper includes both continuous and discrete variables (shunt compensators, VARs).

3.3. Modeling of Wind Turbine Units

When the wind velocity (Γ_v) is measured, Equation (28) serves as a tool to determine the power output P_w from a wind turbine (WT) [33]. This equation provides a method for calculating the energy produced by the turbine based on the specific speed of the wind encountered:

$$P_w(\Gamma_v) = P_{rated} \cdot \frac{\Gamma_v - \Gamma_v^{(Cut\_in)}}{\Gamma_v^{(Rated)} - \Gamma_v^{(Cut\_in)}} \tag{28}$$

where $\Gamma_v^{(Cut\_in)}$ is the minimum wind velocity at which the turbine begins generating electricity; $\Gamma_v^{(Rated)}$ is the wind speed at rated power (P_{rated}). When the wind speed at the wind turbine is below the startup speed or above the cutoff speed, the turbine stops generating electricity, and the power output is 0. This means that under these wind speed conditions, the wind turbine does not produce any power output.

By utilizing the Weibull probability density function $f(\Gamma_v)$ and distribution function $F(\Gamma_v)$ described in Equations (29) and (30), this study accurately describes and predicts the variation and distribution characteristics of wind speed at specific locations. This facilitates the determination of optimal installation sites for wind turbines, with the goal of maximizing wind energy capture and electricity generation efficiency [34]. Moreover, the study employs the bi-variate Weibull distribution, characterized by two parameters, to effectively model wind power generation within the context of renewable energy systems.

$$f(\Gamma_v) = \frac{S}{C^S} \cdot \Gamma_v^{S-1} e^{-\left(\frac{\Gamma_v}{C}\right)^S} \tag{29}$$

$$F(\Gamma_v) = 1 - e^{-\left(\frac{\Gamma_v}{C}\right)^S} \tag{30}$$

where the shape parameter, denoted as k, and the scale parameter, denoted as c, are both fundamental parameters characterizing the Weibull distribution.

4. Improved Acceleration Coefficient-Based Bee Swarm Algorithm

The artificial bee colony algorithm (ABC) is a metaheuristic optimization algorithm inspired by the behavior of honeybees. In this algorithm, a population of artificial bees searches for the optimal solution to a given problem by mimicking the foraging behavior of real bees. The algorithm consists of three main components: employed bees, onlooker bees, and scout bees. The employed bees explore the solution space by exploiting known good solutions, the onlooker bees choose solutions based on the quality of the employed bee solutions, and the scout bees explore new regions of the solution space. Through the collaborative efforts of these bees, the algorithm iteratively improves upon candidate solutions until an optimal or near-optimal solution is found.

4.1. Modeling of ABC Algorithm

The ABC algorithm models three types of bees: employed bees, onlookers, and scouts. The position of a bee represents a possible solution to the optimization problem and the nectar amount corresponds to the quality (fitness) of the solution.

(1) Employed Bees: These bees are associated with specific food sources (i.e., solutions) and search for new, nearby food sources (new solutions).
(2) Onlooker Bees: These bees wait in the hive and choose food sources depending on the information shared by employed bees. They select food sources with a higher probability if those sources have higher nectar (better solutions).
(3) Scout Bees: These bees perform random searches to discover new food sources. This role is taken by an employed bee when its food source is exhausted (i.e., when the solution cannot be improved further).

The Bee Colony Algorithm, also known as the Bee Algorithm, is a population-based search algorithm that mimics the food-foraging behavior of honeybees to find the optimal solution to numerical problems. Here is how it works:

(1) Solution update for employed and onlooker bees: The position update, which represents a solution modification, is given by the following:

$$p_i^{(j)} = p_{i,min}^{(j)} + \varphi \left[p_{i,\max}^{(j)} - p_{i,\min}^{(j)} \right] \tag{31}$$

where $p_i^{(j)}$, $p_{i,min}^{(j)}$, and $p_{i,\max}^{(j)}$ are the new position, current position lower limits, and current position upper limits of the i-th bee on the j-th dimension. φ is a random number between $[-1, 1]$ that controls the perturbation size, influencing how far the new position will be from the current one.

(2) Fitness Evaluation: Each solution's fitness is evaluated to determine its quality. Typically, the fitness function is problem-specific, designed to evaluate how well a given solution meets the optimization objectives.
(3) Probability Selection for Onlooker Bees: Once all the employed bees have searched and evaluated their solutions, they share this information with onlooker bees. Each onlooker bee selects a food source based on a probability $Pb^{(j)}$ proportional to the fitness of the food source:

$$Pb^{(j)} = \frac{\frac{1}{F^j}}{\sum_{j=1}^{N} \frac{1}{F^j}} \tag{32}$$

where F^j is the fitness value of the j-th variable combination. N is the total population size.

(4) Scout Bee Phase: If a food source (solution) cannot be improved further after a certain number of trials (controlled by a parameter called the "limit"), the associated employed bee becomes a scout and abandons the source. The scout bee then randomly generates a new solution, helping to diversify the search and avoid the local optima.

If a bee swarm lacks diversity during the search process, with bees overly concentrated in local regions, they might overlook the global optimum. This issue could stem from restricted search ranges for the bees, compounded by the inherently non-linear, multimodal, and complex nature of the optimization problem, such as power scheduling. These characteristics make the ABC algorithm more prone to falling into local optima. In light of this, this paper proposes the Improved Acceleration Coefficient-based Bee Swarm algorithm (IACBS) to enhance the algorithm's global search capability and address the potential for local optima trapping.

4.2. Modeling of IACBS Algorithm

Due to the fact that the artificial bee colony (ABC) algorithm, despite having three different types of groups, primarily relies on worker bees for the main search process,

the original ABC algorithm's neighborhood search in Equation (31) is based entirely on a random search concept, which lacks a solid foundation. Therefore, the IACBS algorithm modifies the various bee working modes to enhance neighborhood search and avoid premature convergence to local optima.

A. Mathematical model of worker bee operation:

In this paper, the proposed IACBS algorithm aims to enhance the exploration of potentially overlooked search areas by incorporating a repulsion force. This modification allows worker bees to follow the currently identified optimal positions for their search, as specified in Equations (33) and (34). When the randomly generated value rand exceeds the predetermined *pr* value, a reverse search is initiated. The *pr* parameter is set to 0.8 in this study, with *j* representing the worker bee population variable.

$$P_i^{(j)}(k+1) = P_i^{(j)}(k) + sign\begin{bmatrix} \alpha \cdot rand\left(pbest_i^{(j)} - P_i^{(j)}(k)\right) \\ +\beta \cdot rand\left(gbest_i^{(j)} - P_i^{(j)}(k)\right) \end{bmatrix} \tag{33}$$

$$sign = \begin{cases} 1, & \text{if } rand(\cdot) \le pr \\ -1, & \text{else} \end{cases} \tag{34}$$

where α represents the cognitive ability of the worker bee itself, while β denotes the cognitive ability acquired after interacting with other worker bees. $pbest_i^{(j)}$ refers to the best search position of the worker bee itself, while $gbest_i^{(j)}$ is the best search position of the entire worker bee population. *sign* is the criterion for random search by the worker bee. k represents the current iteration number.

The acceleration coefficients in Equation (33) of the worker bee operation model have been modified. Initially, these acceleration coefficients were fixed values set by the user. According to the literature [32], these coefficients are now set as linearly increasing/decreasing variables. The focus of the search is placed near the local optimum region in the early stages of the solution, and near the global optimum region in the later stages. The acceleration coefficients are calculated using Equations (35) and (36).

$$\alpha = (\alpha_f - \alpha_i) \cdot \frac{k}{k_{max}} + \alpha_i \tag{35}$$

$$\beta = (\beta_f - \beta_i) \cdot \frac{k}{k_{max}} + \beta_i \tag{36}$$

Using Equations (35) and (36), Equation (33) is rewritten as Equation (37).

$$P_i^{(j)}(k+1) = P_i^{(j)}(k) + sign\begin{bmatrix} \left(\alpha_f - \alpha_i\right) \cdot \frac{k}{k_{max}} + \alpha_i \cdot rand\left(pbest_i^{(j)} - P_i^{(j)}(k)\right) \\ +\left(\beta_f - \beta_i\right) \cdot \frac{k}{k_{max}} + \beta_i \cdot rand\left(gbest_i^{(j)} - P_i^{(j)}(k)\right) \end{bmatrix} \tag{37}$$

B. Mathematical model of follower bee operation:

The follower bee also uses Equation (32) to determine whether to follow the worker bee for foraging. However, in the IACBS, the worker bee mode is changed to only follow rather than join the worker bee population. In the follower bee operation model, a repulsion force search is also added to increase the search area. The variable z represents the follower bee population variable.

$$P_i^{(z)}(k+1) = P_i^{(z)}(k) + sign\left[\beta \cdot rand\left(P_i^{(e)}(k) - P_i^{(z)}(k)\right)\right] \tag{38}$$

where $P_i^{(e)}$ is the follower position selected through Equation (32), but the variable N in Equation (32) is changed to represent the total number of worker bees.

C. Mathematical model of scout bee operation:

In the IACBS algorithm, the scout bee operation model will no longer involve arbitrary random searches. Instead, the scout bee operation model is modified to generate new positions for scout bees based on comparisons between the global best solution and the average position of the entire group. The variable s represents the scout bee population variable.

$$P_i^{(s)}(k+1) = P_i^{(s)}(k) + sign[rand(gbest_i - \mu \cdot M(k))] \tag{39}$$

$$\mu = round[1 + rand(0,1)] \tag{40}$$

where M is the average position of all the groups at iteration k.

4.3. The IACBS Algorithm Solves the Power Flow Problem

This paper proposes the IACBS algorithm to solve the optimized power flow based on calibrated safety constraints. The system can preemptively adjust and schedule for specific incidents with the highest risk based on the results of optimized power flow. In the event of an accident, it can prevent the power system containing wind turbines from operating in a state that violates constraints without changing any dispatch, ensuring safe operation within limits. The control variables of the system can be divided into continuous variables (the real power output of synchronous generators and wind turbines, and voltage at the generator bus) and discrete variables (parallel capacitor banks). The steps for solving this are as follows:

Step 1: Establish system data

Input the data for the problem, including the transmission line data, parameters of each synchronous generator unit and wind turbine generator unit, and various constraint conditions.

Step 2: Incident analysis

Utilize the ECI load flow and the simplified correction function for generator and transmission line tripping incidents to perform incident analysis. Develop a new safety analysis tool and add new analysis functions. During the execution of safety analysis, unlike traditional methods that are limited to only one or two Newton iterations, the method can directly converge, significantly improving simulation accuracy. Additionally, it can further rank the severity of incidents based on the analysis.

Step 3: Selection of the most severe case for the system

Identify the most severe (congested) case. Suppose that when a line or a generator fails, it causes one of the grid's lines to overload, and this incident leads to a greater overload than other incidents. In this scenario, we select this case as the most severe case. Generally, OPF cannot simultaneously handle the original system (without considering faults) and the system after an incident. Therefore, the IACBS algorithm is introduced to solve this problem.

Step 4: Initialization of the IACBS algorithm

Initialize the population and set the iteration number k = 1. Initialize the population ratio with three types of bee groups and generate the initial positions of the bee groups randomly.

Step 5: Calculation of the fitness function value

Calculate the fitness value according to the objective function, as shown in Equation (32).

Step 6: Selection of *pbest* and *gbest*

Based on the fitness function value, select and record pbest and gbest. If it is not the first iteration, compare and update *pbest* and *gbest*.

Step 7: Find the bee group to which *pbest* belongs

Based on the bee group to which pbest belongs, increase the number of bees in that group and decrease the number of bees in the other groups, ensuring compliance with the specified constraints.

Step 8: Check if the number of bees in each group reaches the maximum limit

If the number of bees in a group reaches the maximum limit, do not record the change in the number of bees, and set $ct = ct + 1$; otherwise, set $ct = 0$. If ct reaches the maximum limit, revert the bee group ratio to the initial ratio.

Step 9: Update the positions of bees in each group

Each bee group will search according to its working mode and update its position, i.e., the equations for worker bees (33) and (37), follower bees (38), and scout bees (39).

Step 10: Check if the maximum number of iterations is reached

Check if the maximum number of iterations is reached. If not, set $k = k + 1$ and return to Step 5 to continue executing. If the maximum number of iterations is reached, output the best solution.

The flowchart of the proposed IACBS algorithm for solving CSCOPF is shown in Figure 2.

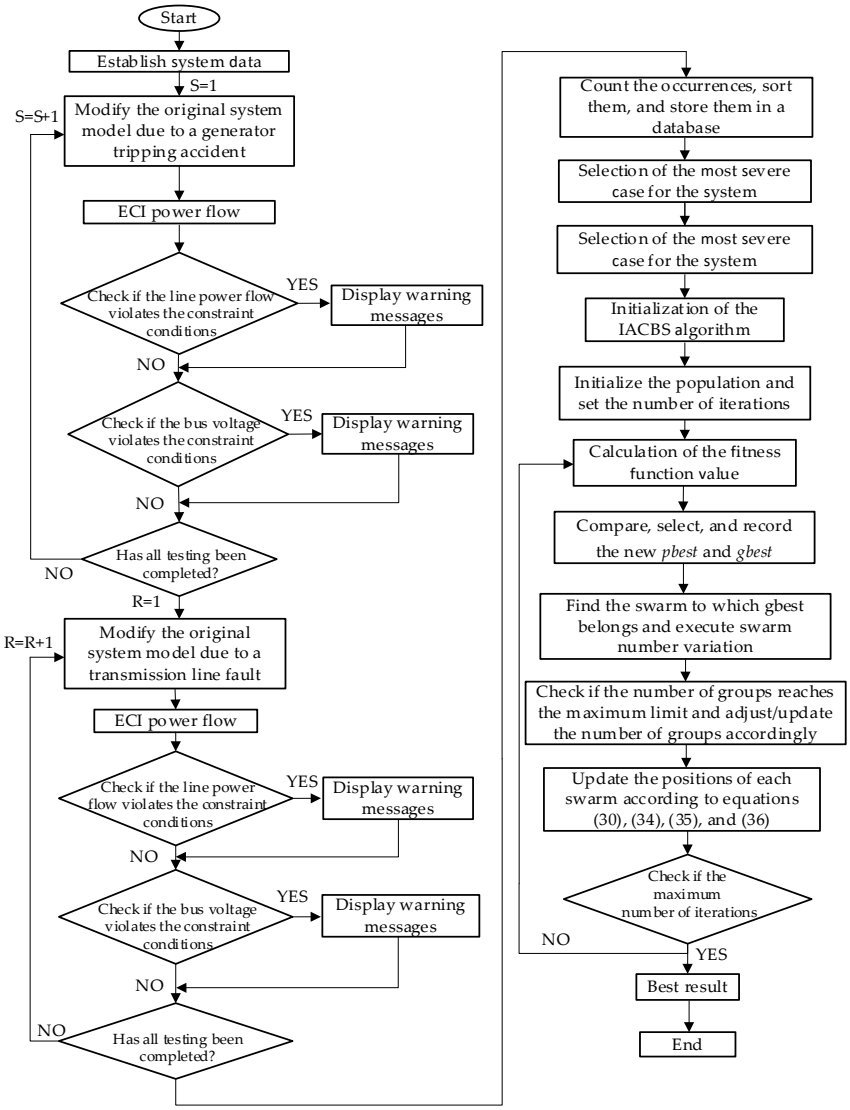

Figure 2. The flowchart of solving CSCOPF.

5. System Testing and Case Analysis

This section evaluates the proposed Calibrated Safety Constraints Optimal Power Flow (CSCOPF) method through comprehensive system testing and case analysis using the IEEE 30-bus system (Figure 3). The system comprises 6 generators, 41 transmission lines, and 9 capacitor banks. Parameters for the generators, bus voltage limits, and transmission line flow limits are sourced from previous studies [32], while wind farms connected to buses 5 and 11 are modeled with rated powers of 75 MW and 60 MW, respectively. The Weibull distribution parameters and average wind speeds for these farms are also included [35]. The objective of this section is to verify the feasibility and performance of the CSCOPF method and to compare the IACBS algorithm with the Genetic Algorithm with Chaos Optimization (GACO) and Modified Particle Swarm Optimization (MPSO) methods to assess its robustness. The research utilized MATLAB R2016b for simulations, conducted on a computer with an i5 CPU clocked at 2.9 GHz and 16 GB of RAM.

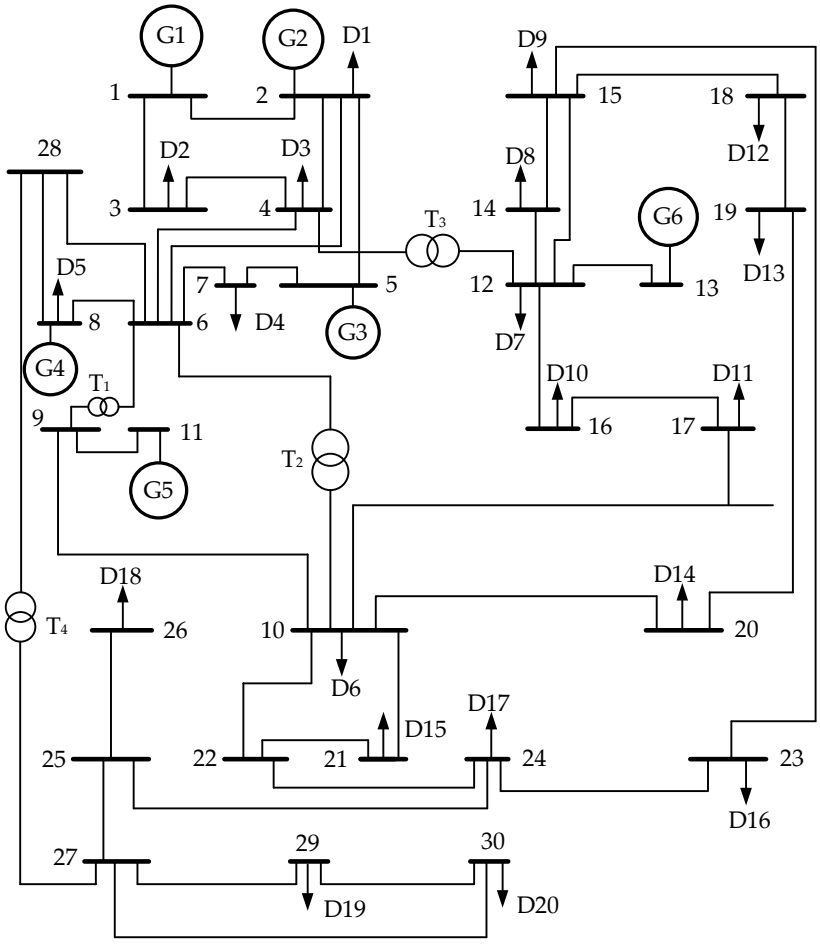

Figure 3. IEEE 30-bus system.

5.1. Case 1: Ignore Contingency Analysis and Do Not Consider Integer Issues in OPF

In this case, the continuous-variable CSCOPF problem was analyzed without considering contingency analysis or integer variables. The objective was to minimize the generation cost while optimizing the active power outputs and voltages of generators. The state variables included the real and imaginary parts of the bus voltages, and the constraints encompassed generator power limits, bus voltage limits, and transmission line capacity limits, with reactive power limits being disregarded. The CSCOPF model ensures that even under normal operational conditions, without fault analysis, the system maintains stable power flow and optimal generator dispatch.

The IACBS algorithm was applied to solve the CSCOPF problem, and it demonstrated superior performance compared to GACO and MPSO. Specifically, IACBS integrated with CSCOPF achieved the lowest generation cost and the fastest convergence. The process involved running 50 test runs to measure performance metrics like execution time, convergence speed, and generation cost, ensuring comparability across different algorithms.

The optimal generation cost achieved by IACBS was USD 487.4315 per hour, with an average solution cost of USD 487.7347 per hour, which was lower than both MPSO's USD 487.7567 per hour and GACO's USD 487.89 per hour. IACBS also demonstrated superior convergence, requiring an average of 179.1 iterations, compared to MPSO (220.7 iterations) and GACO (235.6 iterations). The execution time for IACBS was 92.1 s, significantly faster than MPSO (126.4 s) and GACO (147.8 s). These results clearly highlight the efficiency of CSCOPF when combined with IACBS in maintaining low operational costs even under standard power flow conditions.

Table 1 shows the active power outputs of synchronous generators (G1, G2, G4, and G6) and wind generators (G3 and G5), while Tables 2 and 3 present the optimal power flow distribution, as well as the state of bus complex power and power flow in the OPF analysis, respectively. Figure 4 demonstrates that all the transmission line flows remain within system limits. This confirms that the CSCOPF model, supported by IACBS, ensures system stability and operational safety without the need for contingency analysis. The results also highlight the practical value of CSCOPF in achieving economic efficiency and system stability under typical operational scenarios. Table 4 demonstrates the robust performance of the IACBS algorithm, with shorter execution time, consistent cost outcomes, and fewer iterations compared to GACO and MPSO.The clear steps and performance comparisons make the analysis replicable, further supporting the robustness and practicality of the proposed approach (Figure 5).

Table 1. The OPF result of the synchronous generators and wind generators in case 1.

Parameters	Synchronous Generators/Wind Generators					
	G1	**G2**	**G3**	**G4**	**G5**	**G6**
P_G (MW)	19.257	76.916	21.22	38.425	45.576	30
$\|U_G\|$ (p.u.)	1.0038	1.0934	1.0042	1.0358	1.0061	1.0038

Table 2. State of bus complex power in OPF.

Bus No.	Voltage Level (p.u.)	Degrees (°)	Generator Complex Power (p.u.)	Load Complex Power (p.u.)
1	1.00000	0.00000	0.19257 − j0.09389	0.00000
2	1.00380	−0.19788	0.76916 + j0.26236	0.22785 + j0.12700
3	0.99146	−1.73650	0.00000	0.02520 + j0.01200
4	0.99020	−2.04809	0.00000	0.07980 + j0.01600
5	0.98861	−1.83370	0.38425 + j0.06901	0.00000
6	0.98176	−2.41184	0.00000	0.00000
7	0.97481	−2.75291	0.00000	0.23940 + j0.10900
8	0.96902	−2.92206	0.30000 + j0.09058	0.31500 + j0.30000
9	0.98952	−2.52170	0.00000	0.00000
10	0.99359	−2.57857	0.00000	0.06090 + j0.02000
11	0.98952	−2.52170	0.15576 + j0.11916	0.00000
12	1.03255	−2.78157	0.00000	0.11760 + j0.07500
13	1.09340	−1.27373	0.21220 + j0.47801	0.00000
14	1.01916	−3.19388	0.00000	0.06510 + j0.01600
15	1.02059	−2.76551	0.00000	0.08610 + j0.02500
16	1.00870	−3.00165	0.00000	0.03675 + j0.01800
17	0.99269	−2.93110	0.00000	0.09450 + j0.05800
18	0.99802	−3.47351	0.00000	0.03360 + j0.00900

Table 2. *Cont.*

Bus No.	Voltage Level (p.u.)	Degrees (°)	Generator Complex Power (p.u.)	Load Complex Power (p.u.)
19	0.98837	−3.70021	0.00000	0.09975 + j0.03400
20	0.98874	−3.48049	0.00000	0.02310 + j0.00700
21	0.99854	−2.20990	0.00000	0.18375 + j0.11200
22	1.00420	−1.96189	0.00000	0.00000
23	1.03580	−1.03590	0.00000	0.03360 + j0.01600
24	1.00349	−2.09175	0.00000	0.09135 + j0.06700
25	0.99936	−2.54506	0.00000	0.000000.00000
26	0.98105	−3.02512	0.00000	0.03675 + j0.02300
27	1.00610	−2.53532	0.00000	0.00000
28	0.98221	−2.58483	0.00000	0.00000
29	0.98507	−3.89364	0.00000	0.02520 + j0.00900
30	0.97294	−4.84581	0.00000	0.11130 + j0.01900

Table 3. State of power flow in OPF.

Line No.	Complex Power (p.u.)	Line No.	Complex Power (p.u.)	Line No.	Complex Power (p.u.)	Line No.	Complex Power (p.u.)
$Line_{1-2}$	0.03303 − j0.08924	$Line_{2-1}$	−0.03290 + j0.05953	$Line_{3-1}$	−0.15826 − j0.01034	$Line_{18-15}$	−0.08657 − j0.05872
$Line_{1-3}$	0.15954 − j0.00465	$Line_{16-17}$	0.02489 + j0.07452	$Line_{4-2}$	−0.19177 − j0.01829	$Line_{19-18}$	−0.05265 − j0.04903
$Line_{2-4}$	0.19402 + j0.00479	$Line_{15-18}$	0.08778 + j0.06114	$Line_{4-3}$	−0.13288 + j0.00238	$Line_{20-19}$	0.04717 − j0.01486
$Line_{3-4}$	0.13306 − j0.00166	$Line_{18-19}$	0.05297 + j0.04972	$Line_{5-2}$	−0.15050 − j0.04522	$Line_{20-10}$	−0.07027 + j0.00786
$Line_{2-5}$	0.15173 + j0.03026	$Line_{19-20}$	−0.04710 + j0.01503	$Line_{6-2}$	−0.22520 − j0.05071	$Line_{17-10}$	−0.07010 + j0.01537
$Line_{2-6}$	0.22846 + j0.04079	$Line_{10-20}$	0.07073 − j0.00678	$Line_{6-4}$	−0.19386 − j0.15829	$Line_{21-10}$	0.10271 + j0.02687
$Line_{4-6}$	0.19451 + j0.16089	$Line_{10-17}$	0.07025 − j0.01495	$Line_{7-5}$	−0.14921 − j0.05364	$Line_{22-10}$	0.08615 + j0.03120
$Line_{5-7}$	0.15050 + j0.04712	$Line_{10-21}$	−0.10237 − j0.02608	$Line_{7-6}$	−0.09019 − j0.05536	$Line_{22-21}$	0.28748 + j0.14091
$Line_{6-7}$	0.09053 + j0.04669	$Line_{10-22}$	−0.08557 − j0.02995	$Line_{8-6}$	−0.27173 − j0.23975	$Line_{23-15}$	0.16011 + j0.00115
$Line_{6-8}$	0.27313 + j0.24534	$Line_{21-22}$	−0.28646 − j0.13888	$Line_{9-6}$	−0.00887 + j0.03660	$Line_{24-22}$	−0.01060 + j0.00313
$Line_{6-9}$	0.00887 − j0.03629	$Line_{15-23}$	−0.15772 + j0.00363	$Line_{10-6}$	−0.00507 + j0.02100	$Line_{24-23}$	−0.10427 − j0.06923
$Line_{6-10}$	0.00507 − j0.02074	$Line_{22-24}$	0.01062 − j0.00310	$Line_{11-9}$	0.00000	$Line_{25-24}$	−0.02342 + j0.00108
$Line_{9-11}$	0.00000 + j0.00000	$Line_{23-24}$	0.10629 + j0.07343	$Line_{10-9}$	−0.00887 + j0.03676	$Line_{26-25}$	−0.03675 − j0.02300
$Line_{9-10}$	0.00887 − j0.03660	$Line_{24-25}$	0.02353 − j0.00090	$Line_{12-4}$	−0.05034 + j0.16852	$Line_{27-25}$	0.01391 + j0.02499
$Line_{4-12}$	0.05034 − j0.16098	$Line_{25-26}$	0.03724 + j0.02374	$Line_{13-12}$	0.21220 + j0.47801	$Line_{27-28}$	0.00214 + j0.06009
$Line_{12-13}$	−0.21220 − j0.44598	$Line_{25-27}$	−0.01382 − j0.02482	$Line_{14-12}$	−0.04395 − j0.03212	$Line_{29-27}$	−0.06390 − j0.01520
$Line_{12-14}$	0.04429 + j0.03287	$Line_{28-27}$	−0.00214 − j0.05866	$Line_{15-12}$	−0.03746 − j0.07378	$Line_{30-27}$	−0.07298 − j0.01352
$Line_{12-15}$	0.03792 + j0.07464	$Line_{27-29}$	0.06488 + j0.01706	$Line_{16-12}$	−0.06164 − j0.09252	$Line_{30-29}$	−0.03832 − j0.00548
$Line_{12-16}$	0.06273 + j0.09495	$Line_{27-30}$	0.07484 + j0.01701	$Line_{15-14}$	0.02130 − j0.01599	$Line_{28-8}$	0.04355 + j0.04217
$Line_{14-15}$	−0.02115 + j0.01612	$Line_{29-30}$	0.03870 + j0.00620	$Line_{17-16}$	−0.02440 − j0.07337	$Line_{28-6}$	−0.04142 + j0.01649
$Line_{8-28}$	−0.04327 − j0.06025	$Line_{6-28}$	0.04146 − j0.02600				

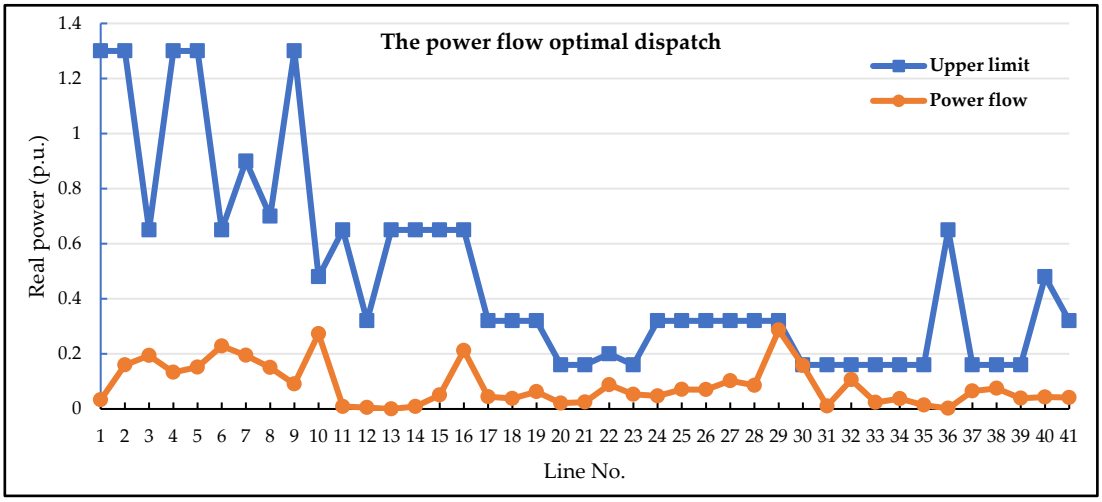

Figure 4. The optimal power flow distribution.

Table 4. Performance comparison of the IACBS algorithm.

Method	Execution Time (s)			Cost (USD/h)			Number of Iterations		
	Max_Time	Min_Time	Avg_Time	Worst	Best	Avg.	Max_Count	Min_Count	Avg_Count
GACO	166.534	97.861	147.842	487.5984	487.4315	487.8900	310	214	235.6
MPSO	141.265	90.681	126.403	487.5691	487.4315	487.7567	286	195	220.7
IACBS	121.905	73.563	92.100	487.5740	487.4315	487.7347	227	85	110.1

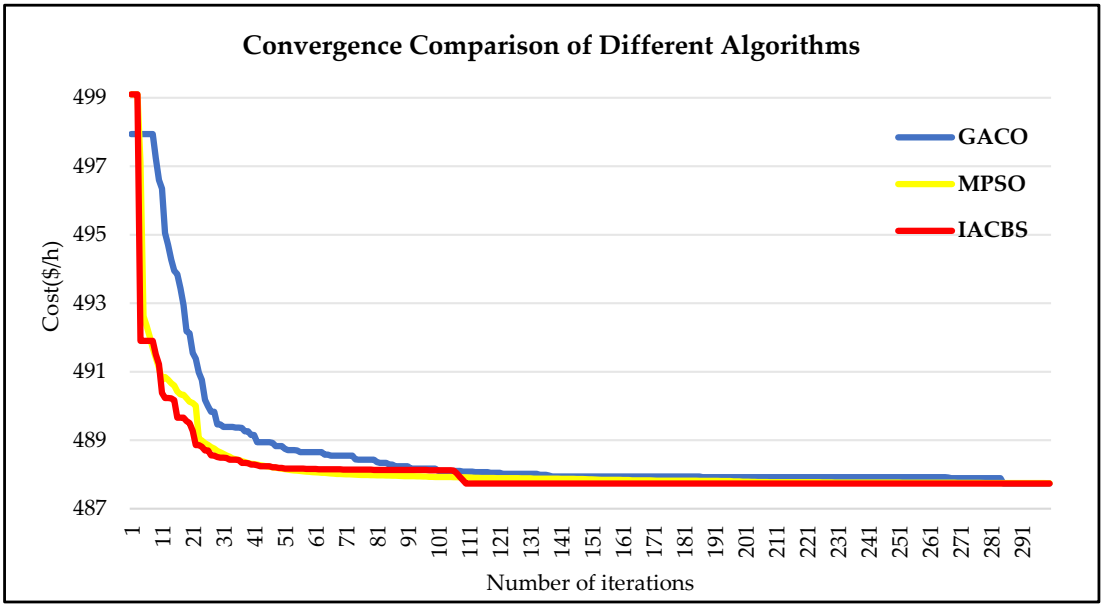

Figure 5. The convergence comparison of different algorithms in case 1.

5.2. Case 2: Considering Contingency Analysis but Ignoring the Integer Aspects of the CSCOPF Problem

In this case, we examine the optimal dispatch for the CSCOPF problem, incorporating contingency analysis while excluding integer variables. The approach begins with conducting a contingency analysis on the IEEE 30-bus system, utilizing the ECI load flow analysis program developed in this study. This program, capable of handling generator and transmission line outages, enhances the system's computational efficiency, reduces memory requirements, and provides robust modeling, thus significantly improving simulation accuracy compared to traditional methods that rely on limited Newton iterations. Table 5 presents the original system data used in the analysis.By integrating the CSCOPF model, this approach ensures that system reliability is maintained, even under severe fault scenarios.

Table 5. Original system data.

Parameters	Synchronous Generators/Wind Generators					
	G1	G2	G3	G4	G5	G6
P_G (MW)	35.82	60.97	37.00	21.59	49.20	26.91
$\|U_G\|$ (p.u.)	1.00	1.00	1.00	1.00	1.00	1.00

The PISA framework involved performing 46 load flow calculations, which were completed in a swift 0.551 s per calculation. The results, detailed in Table 6, rank the potential hazards based on their severity. The most critical scenario identified was a fault on Line 10–22, leading to a significant overload of 4.9134 MW on Line 21–22. This systematic fault analysis highlights the strength of CSCOPF in identifying and mitigating system vulnerabilities before they escalate. The IACBS algorithm, integrated with the

CSCOPF model, was applied to manage the system's response to severe contingencies, optimizing the preventive scheduling process.

Table 6. Severity ranking under PISA.

No.	Faulty Component	Overloaded Transmission Line	Overloaded Power Flow (MW)
1	$Line_{10–22}$	$Line_{21–22}$	4.9134
2	$Line_{6–8}$	$Line_{6–28}$	3.0416
3	$Line_{15–23}$	$Line_{21–22}$	1.641
4	$Line_{4–6}$	$Line_{21–22}$	1.5349
5	$Line_{12–13}$	$Line_{15–23}$	1.5177
6	G1	$Line_{21–22}$	1.3771
7	$Line_{15–18}$	$Line_{21–22}$	0.8459
8	$Line_{2–6}$	$Line_{21–22}$	0.7945
9	$Line_{6–28}$	$Line_{21–22}$	0.6262
10	G2	$Line_{15–23}$	0.5157

Figures 6 and 7 illustrate that the optimal dispatch, derived from the analysis, successfully maintains system stability under both normal and fault conditions. The IACBS algorithm, in conjunction with the CSCOPF model, effectively manages the system's response to severe contingencies, ensuring that voltages and power flows remain within acceptable limits. Even when subjected to the most severe faults, the system operates within safe boundaries, showcasing the robustness of the IACBS algorithm in handling complex scenarios and ensuring system security. This highlights CSCOPF's preventive scheduling capabilities, minimizing risks under fault conditions.

When incorporating the most severe contingency into the CSCOPF framework and solving it using the proposed IACBS algorithm, the optimal dispatch results of CSCOPF, without considering discrete variables (such as ignoring shunt capacitor banks), can be obtained as shown in Table 6. Although the generation cost of CSCOPF is slightly higher than that of OPF without contingency analysis under normal operating conditions, CSCOPF's preventive dispatch strategy ensures system safety during critical contingencies, avoiding system collapse that traditional OPF might lead to in extreme scenarios. According to the comparisons in Figures 6 and 7, the system voltage and power flow under the optimal dispatch of CSCOPF remain within the specified limits, regardless of whether the most severe contingency occurs.

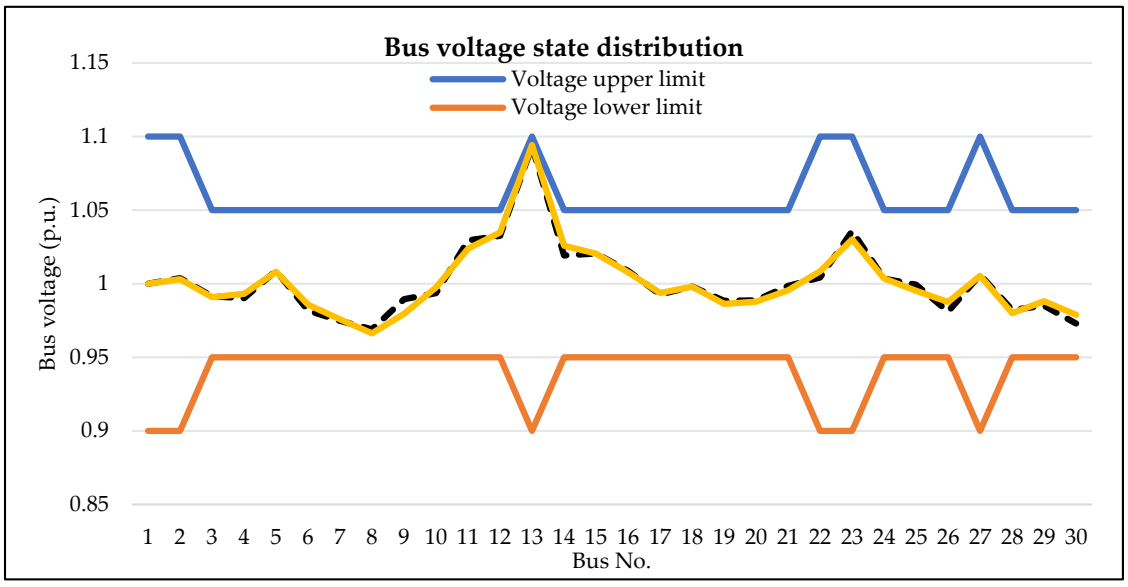

Figure 6. The optimal voltages dispatched during fault conditions in case 2.

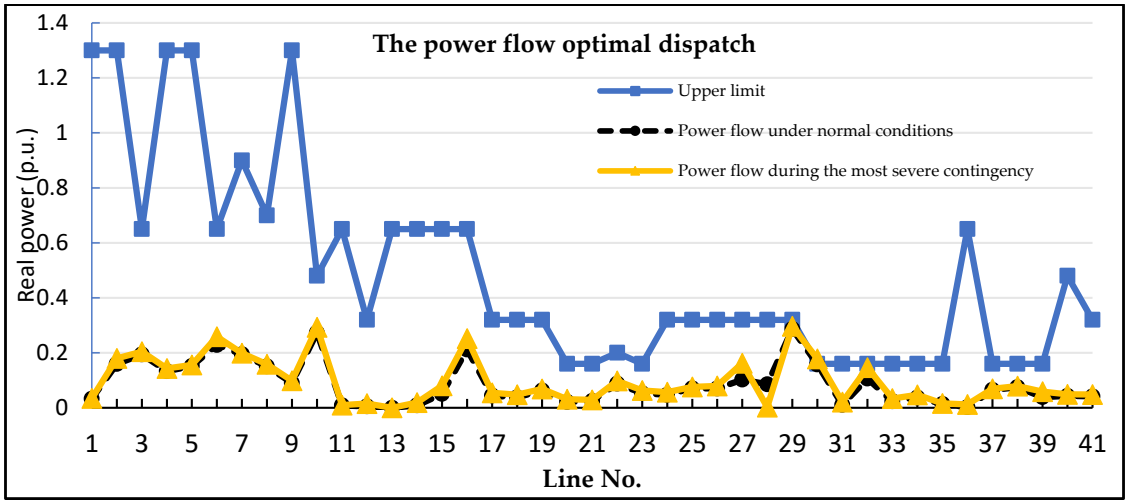

Figure 7. The CSCOPF distribution under normal and the most severe contingency in case 2.

As shown in Table 7, the optimal dispatch results obtained using the IACBS algorithm comply with the generator constraints. Although the active power outputs of synchronous generator 2 (80 MW) and wind farm generator 5 (60 MW) have reached the system's upper limits, they remain within the system's permissible range. Figure 6 indicates that the bus voltages are within the allowable range, both in normal operation and during the most critical contingency, with only the voltage at bus 13 being slightly higher (1.0743 p.u.), but still within the system voltage limit of 1.1 p.u. The other bus voltages perform well. Figure 7 shows that the system power flows are also maintained within limits during both normal and fault conditions, with the power flow on $\text{Line}_{21–22}$ reaching its upper limit. Since the most severe contingency occurs on $\text{Line}_{10–22}$, Figure 7 shows that only the power flows in the nearby region ($\text{Line}_{10–21}$, $\text{Line}_{10–22}$, and $\text{Line}_{21–22}$) exhibit significant changes before and after the fault, while the areas further away are less affected. These results demonstrate that CSCOPF, coupled with IACBS, ensures system stability and maintains power flow within constraints, even in the most critical fault scenarios.

Table 7. The OPF result of the synchronous generators and wind generators in case 2.

Parameters	Synchronous Generators/Wind Generators					
	G1	G2	G3	G4	G5	G6
P_G (MW)	23.342	80.000	20.887	28.151	60.000	19.245
$\lvert U_G \rvert$ (p.u.)	1.0000	1.0031	1.0812	0.9963	1.0239	1.0942

Additionally, the proposed IACBS algorithm demonstrates superior convergence results compared to other stochastic algorithms in the literature under this test scenario, as evident from Table 8. Further comparison of the convergence performance of the three stochastic search algorithms, as illustrated in Figure 8, indicates that the CSCOPF algorithm outperforms the GACO algorithm, while IACBS surpasses CSCOPF. Although IACBS takes longer to converge in this test scenario, it achieves better results. This highlights the superiority of IACBS in addressing multiple constraints and ensuring global optimization, avoiding the local optima that traditional algorithms might fall into. The proposed IACBS overcomes this limitation, showing a higher probability of achieving the global optimum, further demonstrating its robustness.

Table 8. Performance comparison of the IACBS algorithm in case 2.

Method	Execution Time (s)			Cost (USD/h)			Number of Iterations		
	Max_Time	Min_Time	Avg_Time	Worst	Best	Avg.	Max_Count	Min_Count	Avg_Count
GACO	186.166	114.882	149.325	488.9452	487.4421	487.8900	341	245	280.4
MPSO	171.577	101.144	132.723	488.9385	487.4369	487.7912	275	194	211.6
IACBS	211.517	133.395	153.185	488.9371	487.4327	487.7651	287	65	81.9

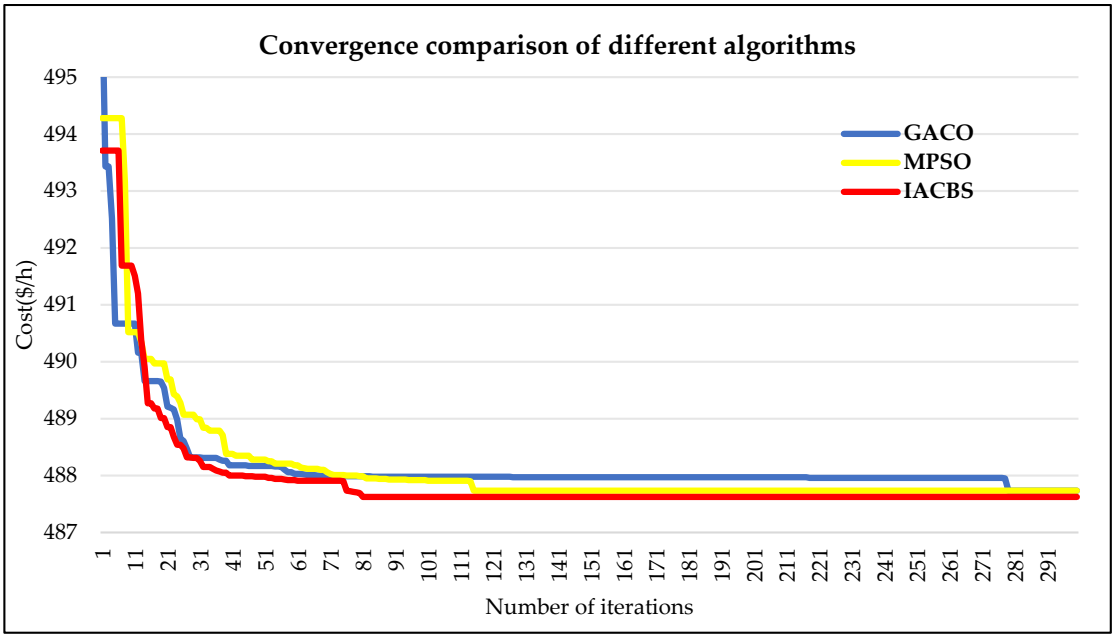

Figure 8. The convergence comparison of different algorithms in case 2.

5.3. Case 3: Considering Contingency Analysis and the Integer Aspects of the CSCOPF Problem

In this case, the study developed a method for solving the CSCOPF problem by incorporating the IACBS algorithm. This approach utilizes the current injection method to control load flow, with the primary objective of minimizing generation costs. The system employs a preventive scheduling strategy, optimized for the most significant potential contingencies, such as a fault on the line between bus 10 and bus 22. This case introduces discrete variables, specifically shunt capacitors with capacities ranging from 0 to 5 MVAR, installed across nine buses with an adjustment step of 1 MVAR. The inclusion of these discrete variables highlights CSCOPF's ability to handle both continuous and discrete variables simultaneously, ensuring system robustness under various conditions.

The results of this case are detailed in Tables 9 and 10. The optimal configuration of shunt capacitors resulted in an operating cost of USD 487.561 per hour, while the worst configuration had an operating cost of USD 488.9431 per hour. The average operating cost across 50 calculations was USD 487.9801 per hour. These results are compared with the performance of the GACO and MPSO algorithms in Table 11 and Figure 9. The results clearly show that CSCOPF integrated with IACBS achieves superior cost efficiency, especially when dealing with discrete variables. The IACBS algorithm, despite requiring a longer convergence time, demonstrated superior performance in terms of cost efficiency and convergence. It effectively managed both continuous and discrete variables, confirming its robustness and ability to handle complex scheduling problems. This robustness ensures that CSCOPF remains an effective solution for power flow optimization even in challenging fault scenarios involving multiple constraints.

Table 9. The optimal dispatch results of CSCOPF in case 3.

Parameters		Synchronous Generators/Wind Generators					
		G1	G2	G3	G4	G5	G6
Best solution	P_G (MW)	21.678	80.000	20.180	31.114	60.000	12.169
	$\|U_G\|$ (p.u.)	1.0000	1.0077	1.0591	1.0046	1.0315	0.99921
	Cost (USD/h)	54.415	200.150	56.747	77.389	60.0507	38.809
Worst solution	P_G (MW)	17.776	75.715	24.101	30.125	60	16.349
	$\|U_G\|$ (p.u.)	1.0000	0.99913	1.0377	0.99400	1.0092	0.99238
	Cost (USD/h)	49.641	194.683	65.708	77.416	60.05	45.845

Table 10. Capacitor optimal and suboptimal configuration.

Shunt No. / Bus No.		1 / 10	2 / 12	3 / 15	4 / 17	5 / 20	6 / 21	7 / 23	8 / 24	9 / 29
Optimal C_{sh} (Mvar)	IACBS	5	4	4	5	5	5	5	4	1
	MPSO	5	1	2	4	5	5	5	5	4
	GACO	5	1	4	5	5	5	4	3	3
Suboptimal C_{sh} (Mvar)	IACBS	3	2	5	5	0	5	5	5	0
	MPSO	4	3	4	5	5	1	0	2	2
	GACO	2	2	1	4	1	5	0	5	3

Table 11. Performance comparison of the IACBS algorithm in case 3.

Method	Execution Time (s)			Cost (USD/h)			Number of Iterations		
	Max_Time	Min_Time	Avg_Time	Worst	Best	Avg.	Max_Count	Min_Count	Avg_Count
GACO	235.860	126.592	217.161	495.9527	487.9116	488.1902	562	121	205.5
MPSO	185.082	93.882	161.156	493.3661	487.9622	488.0521	381	66	180.7
IACBS	200.778	100.371	186.520	488.9431	487.5610	487.9801	287	65	101.9

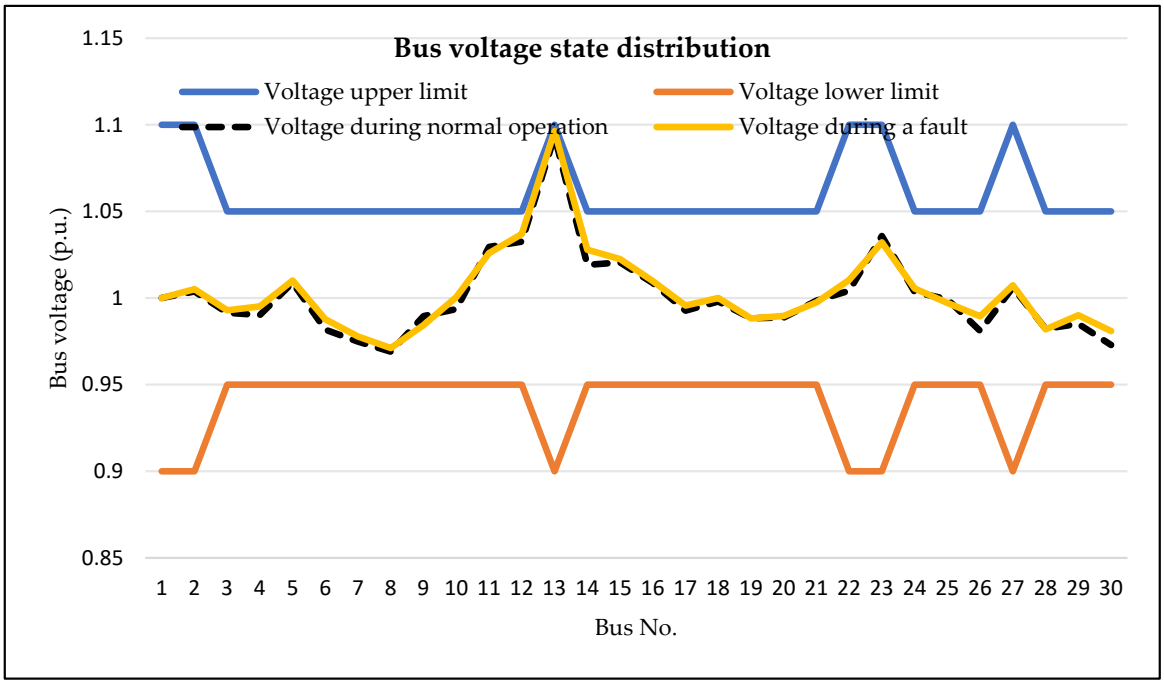

Figure 9. The optimal voltages dispatched during fault conditions in case 3.

The performance comparison illustrates that the IACBS algorithm outperforms both GACO and MPSO in terms of achieving lower costs and faster convergence. This further

emphasizes the strength of the CSCOPF model in optimizing scheduling decisions when integer aspects, such as shunt capacitor configurations, are included. This underscores the effectiveness of IACBS in optimizing scheduling when discrete variables are included, providing a reliable solution for the CSCOPF problem.

The test results indicate that MPSO outperformed GACO in terms of average execution time (161.156 s), average solution (488.0521), and average convergence times (180.7 times). Among these two stochastic search algorithms, IACBS demonstrated superior performance. Figure 9 shows that although MPSO can rapidly approach the optimal solution using Equation (28), relying solely on this equation may lead to fast convergence to a local optimum, failing to find the global optimum. This limitation highlights the importance of CSCOPF's integration with IACBS, which provides a more thorough search process and ensures global optimization. Therefore, in terms of detailed search, Equation (36) provides a mechanism that can escape the local optima and more accurately search for the global optimum.

By applying the optimal scheduling results from Table 9 to the simulated load flow, the system's state during normal operation and under maximum risk conditions was observed, including system voltage conditions before and after faults, as shown in Figure 10, and flow conditions, as shown in Figure 11. This step-by-step approach ensures that CSCOPF's optimization process is clear and replicable. Figures 10 and 11 indicate that under the optimal scheduling of CSCOPF, all voltages and line flows operated within safe limits, whether during normal operation or under maximum risk conditions. This demonstrates the practical effectiveness of CSCOPF in maintaining system stability even in the presence of discrete control elements like shunt capacitors. Except for the automatic adjustment of the swing bus's power output to balance supply and demand, no changes were required in the power output or voltage values of synchronous generators and wind farms, allowing the system to operate normally within safe limits.

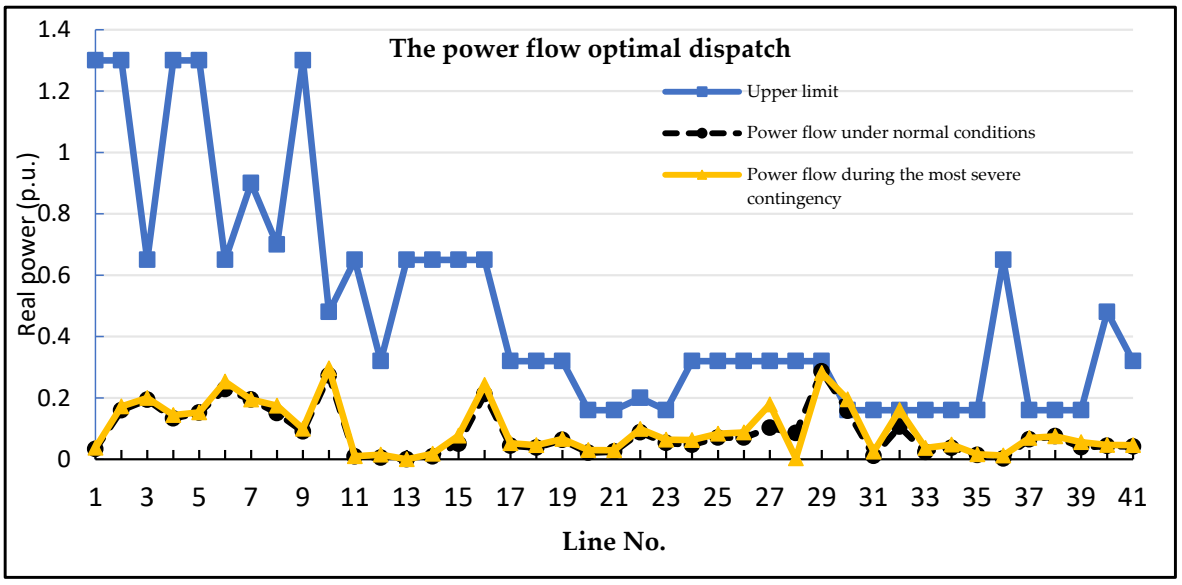

Figure 10. The CSCOPF distribution under normal and the most severe contingency in case 3.

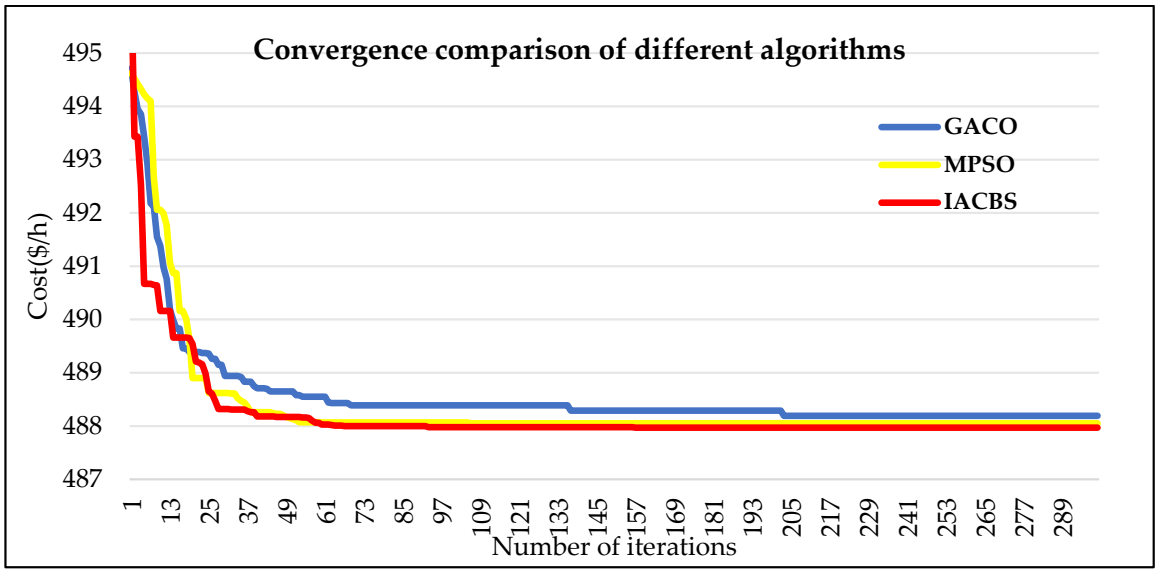

Figure 11. The convergence comparison of different algorithms in case 3.

5.4. The Higher-Order System Test for the IEEE 118-Bus System

To enhance the validation of the proposed method, the IEEE 118-bus system was utilized, which contains 54 generators, 186 transmission lines, and 99 load buses [36]. This system provides a comprehensive platform to assess the method's performance in optimizing power flow and ensuring system stability under various operational conditions, including fault scenarios. The use of such a large-scale system highlights CSCOPF's ability to manage complex power networks efficiently.

In this case, we examine the optimal dispatch for the CSCOPF problem on the IEEE 118-bus system, incorporating contingency analysis. This PISA first conducts a contingency analysis on the IEEE 118-bus system, utilizing the ECI load flow analysis program developed in this study. This program is capable of handling generator and transmission line outages, enhancing system computational efficiency, reducing memory requirements, and providing robust modeling capabilities, thus significantly improving simulation accuracy compared to traditional methods that rely on limited Newton iterations. By integrating CSCOPF with PISA, the system ensures that even under high-risk contingencies, the power flow optimization remains robust and reliable.

The results of the load flow calculations performed by PISA are detailed in Table 12, where the top 10 potential hazards are ranked according to severity. The analysis revealed that the most critical hazard was a fault on Lines 71–72, leading to a significant overload of 13.7591 MW on Lines 69–75. This study focuses on line overloads to determine the most critical cases, intentionally excluding other factors such as voltage deviations to avoid confusion and maintain clarity in the analysis. This method ensures that critical risks are prioritized, allowing the CSCOPF model to mitigate the most severe impacts effectively.

The testing results on the IEEE 118-bus system show that the algorithm successfully minimized generation costs while maintaining stability. The voltage levels remained within the acceptable range during both normal operations and fault conditions. Additionally, the preventive scheduling implemented in the system contributed significantly to its reliability, confirming that the proposed method is applicable to complex and large-scale power networks. This demonstrates CSCOPF's scalability and effectiveness in managing preventive actions across large systems (Figures 12 and 13).

Table 12. Severity ranking under PISA for the IEEE 118-bus system.

No.	Faulty Component	Overloaded Transmission Line	Overloaded Power Flow (MW)
1	$Line_{71–72}$	$Line_{69–75}$	13.7591
2	$Line_{6–8}$	$Line_{90–91}$	8.8512
3	$Line_{1–3}$	$Line_{3–5}$	7.4112
4	$Line_{3–12}$	$Line_{7–12}$	5.8516
5	G2	$Line_{4–5}$	4.5137
6	G21	$Line_{54–55}$	4.1089
7	$Line_{105–108}$	$Line_{105–107}$	3.8519
8	$Line_{100–103}$	$Line_{100–104}$	1.8477
9	G45	$Line_{100–101}$	0.9502
10	G40	$Line_{92–93}$	0.7018

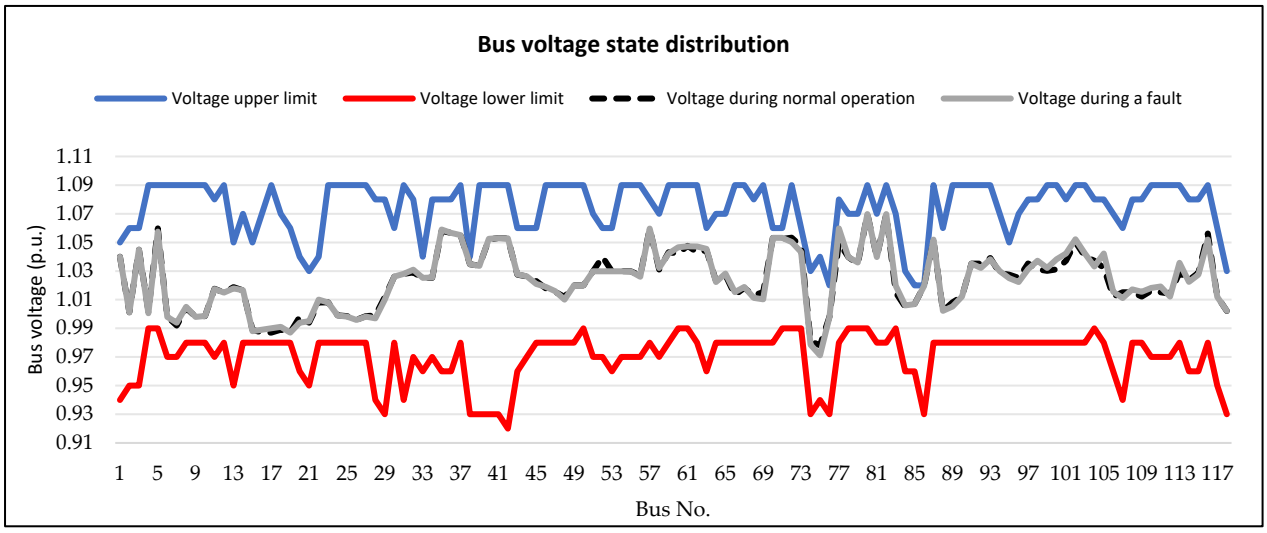

Figure 12. The optimal voltages dispatched during fault conditions for the IEEE 118-bus system.

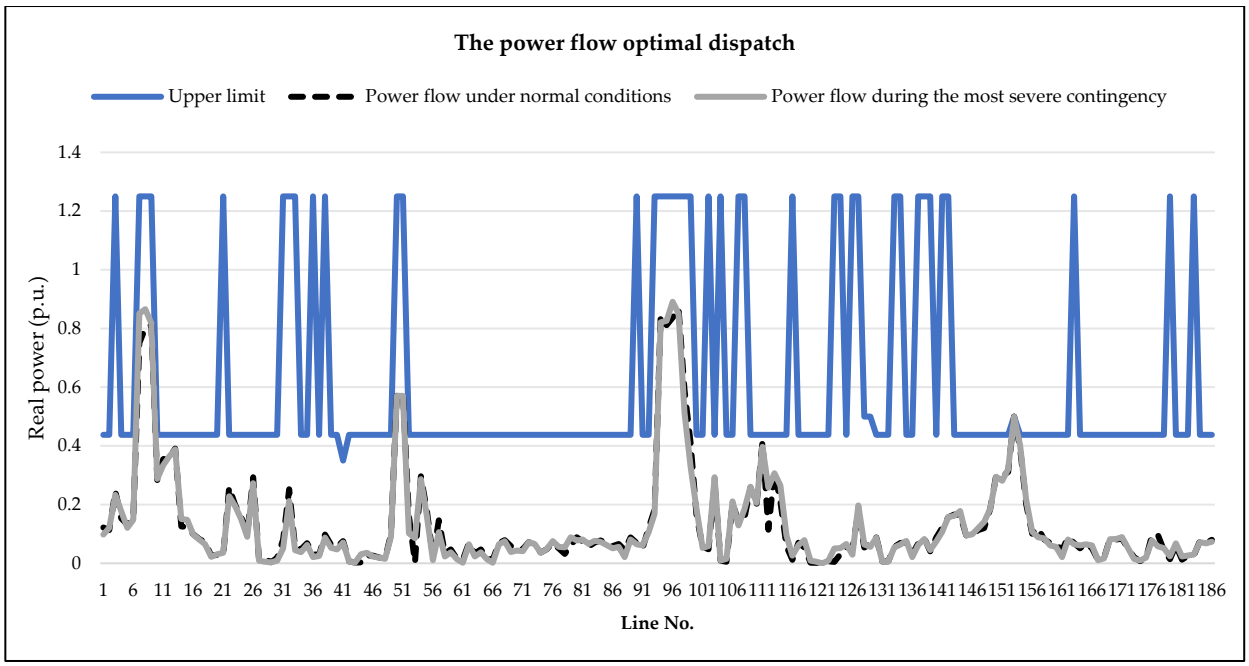

Figure 13. The CSCOPF distribution under normal and the most severe contingency for the IEEE 118-bus system.

The results of this case are detailed in Table 13. The optimal resulted in an operating cost of USD 130,170.96 per hour, while the worst configuration had an operating cost of USD 133,573.08 per hour. The average operating cost across 50 calculations was USD 132,663.57 per hour. These results are compared with the performance of the GACO and MPSO algorithms in Table 13 and Figure 14. The comparison clearly shows that the IACBS algorithm, integrated with CSCOPF, provides superior cost efficiency and stability, even in large-scale power systems. The IACBS algorithm, despite requiring a longer convergence time, demonstrated superior performance in terms of cost efficiency and convergence. It effectively managed the variables, confirming its robustness and ability to handle complex scheduling problems. The algorithm's ability to escape the local optima and find global solutions, even in larger networks like the IEEE 118-bus system, underscores its practical applicability.

Table 13. The optimal dispatch results of CSCOPF for the IEEE 118-bus system.

Method	Execution Time (s)			Cost (USD/h)			Number of Iterations		
	Max_Time	Min_Time	Avg_Time	Worst	Best	Avg.	Max_Count	Min_Count	Avg_Count
GACO	357.052	114.07	297.445	133,511.91	132,055.18	132,727.84	605	116	287.0
MPSO	389.258	187.211	350.889	134,107.55	130,170.96	132,681.60	476	134	290.0
IACBS	360.217	190.591	321.029	133,573.08	128,884.57	132,663.57	405	121	299.0

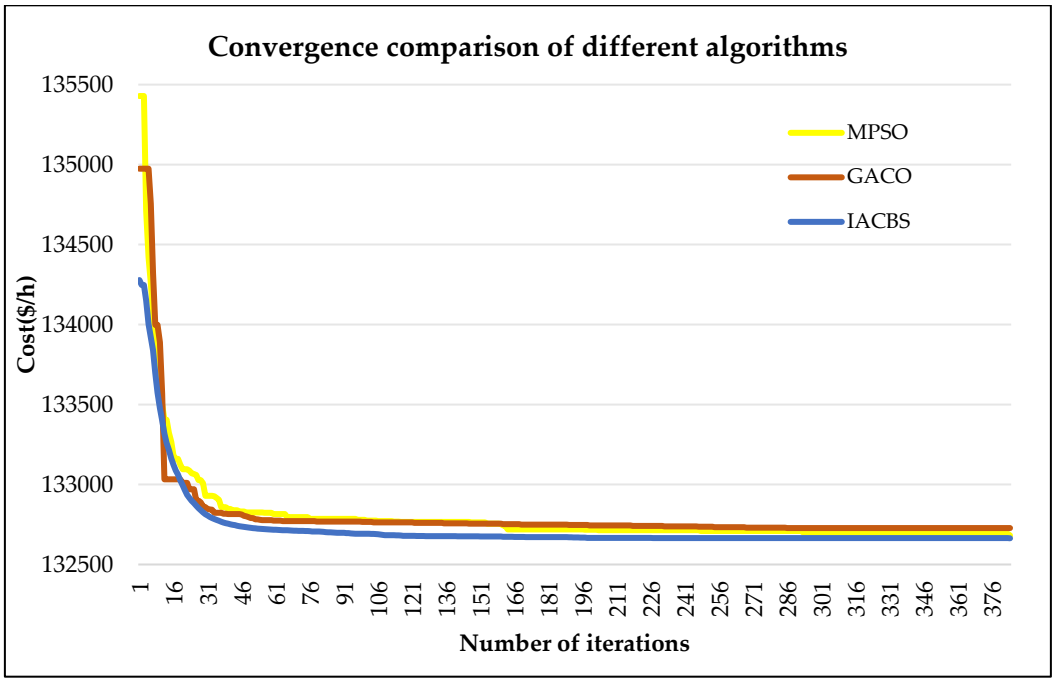

Figure 14. The convergence comparison of different algorithms for the IEEE 118-bus system.

6. Conclusions and Suggestion

6.1. Summary

This study introduced and evaluated the Calibrated Safety Constraints Optimal Power Flow (CSCOPF) method, employing the Improved Acceleration Coefficient-Based Bee Swarm Algorithm (IACBS). Several key objectives were addressed, and the findings are summarized as follows:

The primary objective was to minimize the fuel cost of energy units while optimizing power flow within the system. The results showed that the CSCOPF model effectively reduced generation costs, achieving an optimal cost of USD 487.4315 per hour. The IACBS algorithm demonstrated superior performance in this regard, offering the lowest cost and the fastest convergence speed compared to alternative methods such as GACO and MPSO.

Another critical focus was the impact of integrating wind turbines on system performance. The study revealed that adding wind turbines significantly influences voltage levels and power flows. The equivalent current injection (ECI) method accurately modeled these effects, enabling the optimization process to accommodate the variability introduced by wind power generation.

Furthermore, the effectiveness of the proposed model was evaluated under various operational scenarios, including contingencies and the inclusion of integer variables. The CSCOPF model proved robust in managing these scenarios, maintaining system stability under severe fault conditions, and optimizing the scheduling of discrete variables, such as shunt capacitors. This ensures that the system remains operational and within safe limits even during critical contingencies.

In summary, the IACBS algorithm exhibited superior performance in terms of solution quality and computational efficiency. The CSCOPF method enhances the safety and stability of power systems, particularly under extreme conditions. This approach not only fulfills the study's objectives but also provides a reliable framework for managing complex power systems effectively.

6.2. Practical Applications and Recommendations

Based on the findings of this study, the following practical applications and recommendations are proposed:

1. Integration of wind power with system optimization:

The research demonstrates the effectiveness of the Calibrated Safety Constraints Optimal Power Flow (CSCOPF) method in managing the integration of wind power into the grid. Utilities and grid operators can apply the CSCOPF model to optimize power dispatch and reduce generation costs while ensuring system stability. This approach is particularly useful for grid systems with high renewable energy penetration, providing a robust framework for managing variable wind power outputs.

2. Preventive scheduling for contingency management:

The study's findings highlight the importance of preventive scheduling to handle potential contingencies. Power system operators can use the developed methodology to perform contingency analysis and implement preventive measures, such as adjusting generator outputs and optimizing capacitor settings. This proactive approach can help mitigate the impact of unexpected faults and enhance the overall system reliability.

3. Application of discrete variables in power flow optimization:

The incorporation of discrete variables, such as shunt capacitors, into the optimization process is shown to improve system performance. Grid operators should consider integrating discrete control elements into their optimization models to achieve better cost efficiency and system stability. The results suggest that optimizing the placement and sizing of capacitors can significantly enhance power flow management and system resilience.

4. Enhanced modeling for real-time applications:

The use of the ECI load flow analysis program provides high computational efficiency and robustness. This tool can be adapted for the real-time monitoring and control of power systems. By implementing real-time analysis capabilities, utilities can better respond to dynamic changes in system conditions and maintain optimal performance.

These recommendations provide a practical framework for applying the results of this research to real-world power system management. By implementing these suggestions, utilities and grid operators can enhance system efficiency, stability, and cost-effectiveness.

Author Contributions: K.-H.L. played a key role in the development of the algorithm by conducting research and designing the framework, as well as proposing innovative concepts and applications. W.Q. contributed to fine-tuning the program and validating the simulation outcomes. Y.J. assisted in data analysis and reviewing the draft. Y.-S.Z., besides drafting the initial version of the manuscript, which is set for publication, was responsible for fine-tuning the program, analyzing the data, validating the simulation outcomes, and reviewing the draft. All authors have read and agreed to the published version of the manuscript.

Funding: The project was supported by the Natural Science Foundation of Fujian Province of China (No. 2021J01531) and the Technology Innovation Team of Minnan University of Science and Technology (No. 23XTD112).

Data Availability Statement: Data are contained within the article.

Conflicts of Interest: The authors declare no conflicts of interest.

Nomenclature

P	Active power
Q	Reactive power
V	Voltage magnitude
θ	Voltage angle
I	Current
Z	Impedance
f	Frequency
IACBS	Improved Acceleration Coefficient-Based Bee Swarm Algorithm
CSCOPF	Calibrated Safety Constraints Optimal Power Flow
PISA	Power Incident Safety Analysis
E	Electromotive force
ΔP	Power mismatch
S	Apparent power
T	Time
R	Resistance of transmission line
L	Inductance of transmission line
C	Capacitance of transmission line
G_{SR}	Conductance between buses
B_{SR}	Susceptance between buses
B_C	Capacitive susceptance of transmission line to ground
ΔI_i	Imaginary component of current difference
ΔI_r	Real component of current difference
U_r, U_i	Real and imaginary parts of bus voltages
J	Jacobian matrix (used in Newton–Raphson method)
X	Reactance
Y	Admittance
P_{max}	Maximum active power output
P_{min}	Minimum active power output
λ	Lagrange multiplier

References

1. Lu, K.H.; Rao, Q. Enhancing the Dynamic Stability of Integrated Offshore Wind Farms and Photovoltaic Farms Using STATCOM with Intelligent Damping Controllers. *Sustainability* **2023**, *15*, 13962. [CrossRef]
2. Lu, K.H.; Hong, C.M.; Cheng, F.S. Enhanced Dynamic Performance in Hybrid Power System Using a Designed ALTS-PFPNN Controller. *Energies* **2022**, *18*, 8263. [CrossRef]
3. Yunus, Y.; Özgür, C.; Adnan, T.; Kamil, C.B.; Ümit, C.; Merden, Y.; Mevlüt, A.; Gibran, D.A.T.; Sanjay, K.C.; Josep, M.G.; et al. Impacts of Large-Scale Offshore Wind Power Plants Integration on Turkish Power System. *IEEE Access* **2022**, *10*, 83265–83280.
4. Li, P.; Wu, W.; Wang, X.; Xu, B. A Data-Driven Linear Optimal Power Flow Model for Distribution Networks. *IEEE Trans. Power Syst.* **2023**, *38*, 956–959. [CrossRef]
5. Amr, K.K.; Almoataz, Y.A.; Makram, R.E.; Adel, E.S.; Mahmoud, A.A. Optimal power flow solution of wind-integrated power system using novel metaheuristic method. *Energies* **2021**, *14*, 6117. [CrossRef]
6. Li, S.; Gong, W.; Wang, L.; Yan, X.; Hu, C. Optimal power flow by means of improved adaptive differential evolution. *Energy* **2020**, *198*, 117314. [CrossRef]

7. Khan, I.U.; Javaid, N.; Gamage, K.A.A.; Taylor, C.J.; Baig, S.; Ma, X. Heuristic algorithm based optimal power flow modelincorporating stochastic renewable energy sources. *IEEE Access* **2020**, *8*, 148622–148643. [CrossRef]
8. Xiaoqing, B.; Liyan, Q.; Wei, Q. Robust AC optimal power flow for power networks with wind power generation. *IEEE Trans. Power Syst.* **2016**, *31*, 4163–4164.
9. Chowdhury, M.M.U.T.; Sukumar, K.; Sumit, P. Second-Order Cone Programming (SOCP) Model for Three Phase Optimal Power Flow (OPF) in Active Distribution Networks. *IEEE Trans. Smart Grid* **2023**, *14*, 3732–3743. [CrossRef]
10. Chowdhury, M.M.U.T.; Sukumar, K.; Sumit, P. A Second-Order Cone Programming (SOCP) Based Optimal Power Flow (OPF) Model with Cyclic Constraints for Power Transmission Systems. *IEEE Trans. Power Syst.* **2024**, *39*, 1032–1043. [CrossRef]
11. Morshed, M.J.; Hmida, J.B.; Fekih, A. A probabilistic multi-objective approach for power flow optimization in hybrid wind–PV–PEV systems. *Appl. Energy* **2018**, *211*, 1136–1149. [CrossRef]
12. Shi, L.; Wang, C.; Yao, L.; Ni, Y.; Bazargan, M. Optimal power flow solution incorporating wind power. *IEEE Syst. J.* **2011**, *6*, 233241. [CrossRef]
13. Momoh, J.A.; Adapa, R.; El-Hawary, M.E. A review of selected optimal power flow literature to 1993. I. Nonlinear and quadratic programming approaches. *IEEE Trans. Power Syst.* **1999**, *14*, 96–104. [CrossRef]
14. Pourakbari-Kasmaei, M.; Mantovani, J.R.S. Logically constrained optimal power flow: Solver-based mixed-integer nonlinear programming model. *Int. J. Electr. Power Energy Syst.* **2018**, *97*, 240–249. [CrossRef]
15. Cheng, F.; Liang, H.; Niu, B.; Zhao, N.; Zhao, X. Adaptive Neural Self-Triggered Bipartite Secure Control for Nonlinear MASs Subject to DoS Attacks. *Inf. Sci.* **2023**, *631*, 256–270. [CrossRef]
16. Tang, F.; Wang, H.; Chang, X.-H.; Zhang, L.; Alharbi, K.H. Dynamic event-triggered control for discrete-time nonlinear Markov jump systems using policy iteration-based adaptive dynamic programming. *Nonlinear Anal. Hybrid Syst.* **2023**, *49*, 101338. [CrossRef]
17. Ben Hmida, J.; Javad Morshed, M.; Lee, J.; Chambers, T. Hybrid imperialist competitive and grey wolf algorithm to solve multiobjective optimal power flow with wind and solar units. *Energies* **2018**, *11*, 2891. [CrossRef]
18. Cheng, Y.; Niu, B.; Zhao, X.; Zong, G.; Ahmad, A.M. Event-triggered adaptive decentralised control of interconnected nonlinear systems with Bouc-Wen hysteresis input. *Int. J. Syst. Sci.* **2023**, *54*, 1275–1288. [CrossRef]
19. Zhang, H.; Zhao, X.; Zong, G.; Xu, N. Fully distributed consensus of switched heterogeneous nonlinear multi-agent systems with bouc-wen hysteresis input. *IEEE Trans. Netw. Sci. Eng.* **2022**, *9*, 4198–4208. [CrossRef]
20. Avvari, R.K.; DM, V.K. A Novel Hybrid Multi-Objective Evolutionary Algorithm for Optimal Power Flow in Wind, PV, and PEV Systems. *J. Oper. Autom. Power Eng.* **2022**, *11*, 130–143.
21. Abd-El Wahab, A.M.; Kamel, S.; Hassan, M.H.; Mosaad, M.I.; AbdulFattah, T.A. Optimal Reactive Power Dispatch Using a Chaotic Turbulent Flow of Water-Based Optimization Algorithm. *Mathematics* **2022**, *10*, 346. [CrossRef]
22. Deb, S.; Houssein, E.H.; Said, M.; Abdelminaam, D.S. Performance of turbulent flow of water optimization on economic load dispatch problem. *IEEE Access* **2021**, *9*, 77882–77893. [CrossRef]
23. Jabr, R.A. A conic quadratic format for the load flow equations of meshed networks. *IEEE Trans. Power Syst.* **2007**, *22*, 2285–2286. [CrossRef]
24. Lin, W.M.; Huang, C.H.; Zhan, T.S. A Hybrid Current-Power Optimal Power Flow Technique. *IEEE Trans. Power Syst.* **2008**, *23*, 177–185. [CrossRef]
25. Pareek, P.; Nguyen, H.D. Gaussian Process Learning-Based Probabilistic Optimal Power Flow. *IEEE Trans. Power Syst.* **2021**, *36*, 541–544. [CrossRef]
26. Huang, L.; Lai, C.S.; Zhao, Z.; Yang, G.; Zhong, B.; Lai, L.L. Robust N-k Security constrained Optimal Power Flow Incorporating Preventive and Corrective Generation Dispatch to Improve Power System Reliability. *CSEE J. Power Energy Syst.* **2023**, *9*, 351–364.
27. Liu, H.; Zhang, X.; Wang, Y.; Xu, Y. An Improved Current Injection Model for Power Flow Calculations in Unbalanced Systems. *IEEE Trans. Power Syst.* **2019**, *34*, 1545–1554.
28. Zhang, Y.; Li, G.; Wang, Z.; Liu, Y. A Hybrid Genetic Algorithm for the Economic Dispatch of Power Systems with Wind-Thermal Generation. *Energy Rep.* **2020**, *6*, 1219–1228.
29. Abdo, M.; Kamel, S.; Ebeed, M.; Yu, J.; Jurado, F. Solving Non-Smooth Optimal Power Flow Problems Using a Developed Grey Wolf Optimizer. *Energies* **2018**, *11*, 1692. [CrossRef]
30. Salkuti, S.R. Optimal Power Flow Using Multi-Objective Glowworm Swarm Optimization Algorithm in a Wind Energy Integrated Power System. *Int. J. Green Energy* **2019**, *16*, 1547–1561. [CrossRef]
31. Pham, L.H.; Dinh, B.H.; Nguyen, T.T. Optimal power flow for an integrated wind-solar-hydro-thermal power system considering uncertainty of wind speed and solar radiation. *Neural Comput. Appl.* **2022**, *34*, 10655–10689. [CrossRef]
32. Ahmad, M.; Javaid, N.; Niaz, I.A.; Almogren, A.; Radwan, A. A Bio-Inspired Heuristic Algorithm for Solving Optimal Power Flow Problem in Hybrid Power System. *IEEE Access* **2021**, *9*, 159809–159826. [CrossRef]
33. Mohammadi, F.; Jurado, F. Optimal Power Flow Incorporating FACTS Devices and Stochastic Wind Power Generation Using Krill Herd Algorithm. *Electronics* **2020**, *9*, 1043. [CrossRef]
34. Alghamdi, A.S. Optimal Power Flow of Hybrid Wind/Solar/Thermal Energy Integrated Power Systems Considering Costs and Emissions via a Novel and Efficient Search Optimization Algorithm. *Appl. Sci.* **2023**, *13*, 4760. [CrossRef]

35. Biswas, P.P.; Suganthan, P.N.; Amaratunga, G.A.J. Optimal Power Flow Solutions Incorporating Stochastic Wind and Solar Power. *Energy Convers. Manag.* **2017**, *148*, 1194–1207. [CrossRef]
36. Ali, A.; Abbas, G.; Keerio, M.U.; Touti, E.; Ahmed, Z.; Alsalman, O.; Kim, Y.-S. A Bi-Level Techno-Economic Optimal Reactive Power Dispatch Considering Wind and Solar Power Integration. *IEEE Access* **2023**, *11*, 62799–62819. [CrossRef]